Boosting the host immune system to fight tuberculosis

Boland, R.

5

Host-directed therapy with Amiodarone restricts mycobacterial infection and enhances reactive nitrogen levels, autophagy and lysosomal activity

Ralf Boland[1], Nils Olijhoek[1], Gabriel Forn-Cuní[1], Matthias T. Heemskerk[2], Tom H. M. Ottenhoff[2], Herman P. Spaink[1], Michiel van der Vaart[1*], Annemarie H. Meijer[1*]

1. Institute of Biology Leiden, Leiden University, Leiden, The Netherlands
2. Department of Infectious Diseases, Leiden University Medical Center, Leiden, The Netherlands

* Equal contribution

Manuscript in preparation

Abstract

There is growing concern about the rise of bacterial pathogens becoming resistant to antibiotics. Infection by the pathogen *Mycobacterium tuberculosis*, the causative agent of tuberculosis (TB), is a prime example where antibiotic treatments are losing effectivity. The loss of antibiotic effectivity has raised interest in the identification of host-directed therapeutics (HDTs) to develop novel treatment strategies for TB. In this study we investigated Amiodarone as an HDT drug candidate, which was identified by its antimicrobial effect in a screen of autophagy-modulating compounds. We used the zebrafish embryo model of TB, based on infection with its natural pathogen *Mycobacterium marinum*, to study the host mechanisms involved in the anti-mycobacterial effect of Amiodarone. We show that Amiodarone does not affect mycobacterial growth in culture at the concentrations used, thereby confirming that Amiodarone acts by a host-mediated effect in the zebrafish embryo model of TB. As Amiodarone is known to cause nitric oxide release, we investigated its effect on the reactive nitrogen host defence pathway We detected enhanced activity in both macrophages and neutrophils, although not necessarily colocalizing with mycobacteria. We then used transcriptome analysis and functional assays which indicated that Amiodarone alters host pathways related to autophagy and lysosomal function. In conclusion, we have identified Amiodarone as a strong candidate for further development as an anti-mycobacterial HDT that modulates several innate host defence processes.

Introduction

Tuberculosis (TB) is caused by the intracellular pathogen *Mycobacterium tuberculosis* (*Mtb*). During *Mtb* infection, there is an intricate interplay between the immune system and *Mtb*. On an intracellular level, *Mtb* is capable of resisting destruction by professional phagocytes by manipulation of host pathways[1–3]. On a cellular level this results in the hallmark pathology of TB, the formation of granulomatous aggregates of leukocytes[4]. TB is difficult to treat with classical antibiotics due the presence of dormant bacteria inside TB granulomas that are far less susceptible to antibiotics[5,6]. The rise of infections with multi-drug resistant (MDR) and extensively-drug resistant (XDR) *Mtb* strains is further complicating the treatment of TB[7]. Host-directed therapeutics (HDTs) offer new treatment strategies, even in the case of MDR- and XDR-*Mtb* strains, by enhancing the immune system to combat infection (chapter 1, chapter 3)[8–12]. Largescale genetic and chemical screens of *Mtb*-infected cultured cells have recently reported on a broad spectrum of potential HDTs affecting cellular processes such as lipid metabolism, inflammation and autophagy. During an *in vitro* screen of an autophagy modulating compound library using *Mtb* infected human cells, Amiodarone (Amiodarone-HCl, Sigma-Aldrich) was found to reduce bacterial burden. These results were subsequently reproduced in an *in vivo* screen using the zebrafish (*Danio rerio*) model, making Amiodarone a potentially highly interesting HDT (chapter 3). Here we aim to elucidate via which mechanism Amiodarone is able to restrict mycobacterial infection.

Amiodarone is currently used as antiarrhythmic medication and functions by blocking calcium, sodium and potassium channels as well as inhibiting alpha- and beta-adrenergic receptors. Amiodarone has never been shown to have anti-mycobacterial effects. However, Amiodarone can induce autophagy[13–15]. This intracellular degradation pathway is vital to maintaining homeostasis by removing unwanted elements from the cell, such as misfolded protein aggregates, damaged organelles, and microbial invaders[16,17]. Amiodarone accumulates in acidic organelles and therefore may interact not only with the autophagic pathway but also with other intracellular degradation

processes, like the endocytic pathway[18]. Furthermore, Amiodarone stimulates nitric oxide (NO) release[19]. NO release causes vasodilation and is argued to be an explanation for the cardiovascular protective effects exhibited by Amiodarone[19]. NO is also a key player in immunity and inflammation[20]. Consequently, the effects of Amiodarone on both autophagy and nitric oxide are highly relevant in the context of the host immune response to mycobacterial infection.

Macrophages are the main innate immune cell type that internalize and attempt to eliminate *Mtb* in a process whereby *Mtb*-containing phagosomes mature and fuse with lysosomes. This process results in degradation of the content of the formed phagolysosomes by lysosomal hydrolytic enzymes[1]. However, mycobacteria are remarkably resistant to the host immune system and can manipulate cellular signalling pathways in favour of their own survival. Mycobacteria can arrest phagosome maturation and subsequently escape into the cytosol. After escape, intracellular bacteria are targeted by the autophagy pathway. Inducing autophagy in *Mtb*-infected macrophages has been shown to restrict intracellular bacterial growth, supporting studies into autophagy as a potential target for HDTs against TB[17,21,22]. This led us to investigate if the autophagy-inducing properties of Amiodarone could be the underlying mechanism responsible for the host-directed effect of Amiodarone against TB.

It is known that Amiodarone can induce autophagy in two ways, although the precise mechanisms of action of Amiodarone on the autophagy machinery remain unclear. Firstly, Amiodarone inhibits the function of mTORC1[23]. This complex inhibits autophagy when cellular nutrients are replete by interacting directly with ULK1, which is important for initiation of autophagosome biogenesis[16]. Amiodarone potentially acts via an upstream target in the mTORC1 pathway, as the effect of Amiodarone on autophagosome biogenesis was not immediate after treatment[23]. Secondly, Amiodarone can inhibit autophagy in an mTORC-independent manner by blocking calcium channels and calcium dependent calpains[23]. Calpains inhibit autophagy via stimulation of production of cAMP, which was shown to inhibit autophagy[24,25]. Furthermore, calpains are implicated in the cleavage of Atg5, an important player in the autophagy pathway which is required for the formation of autophagosomes[26]. Interestingly, by potentially interacting with multiple players from the autophagy machinery, Amiodarone might prove to be a robust activator for autophagy in varying conditions, including during infection by mycobacterial pathogens.

Another way via which the host immune system combats intracellular bacterial infection is the formation of reactive oxygen species (ROS), as well as reactive nitrogen species (RNS) that are derived from nitric oxide (NO)[20,27]. NO is formed when L-Arginine is oxidized by nitric oxide synthases (NOS) and can react with superoxide to form peroxynitrite, which has strong antimicrobial activity. There are three NOS enzymes, two of which are constitutively active (neuronal NOS and endothelial NOS) and one is inducible (iNOS) in response to infection and inflammation[20,28]. Although mycobacteria are able to counteract ROS efficiently, they are highly susceptible to RNS[29,30]. Furthermore, it was shown that iNOS defective mice were highly susceptible to *Mtb*[28,31]. Indeed, increased production of RNS associated with increased levels of nitric oxide is host protective[32,33]. Although it is not known how Amiodarone induces NO release, this is another possible mechanism that could explain the beneficial effect of Amiodarone treatment in the context of mycobacterial infection.

In this study we used the zebrafish (*Danio rerio*) model to study the anti-mycobacterial effects of Amiodarone in an *in vivo* model and to elucidate via which host pathways this effect is exerted. The zebrafish embryo model for TB has generated considerable insight in processes involved in the early stages of TB pathogenesis, such as inflammation infection-inducible autophagy and cell death mechanisms[34,35]. In this model, zebrafish

embryos are infected with the close *Mtb* relative *Mycobacterium marinum* (*Mm*) that shares major virulence factors with *Mtb*. The hallmark pathology of TB, the formation of granulomatous aggregates of leukocytes, is recapitulated in zebrafish during *Mm* infection[4,35,36]. We have previously demonstrated that both autophagy and nitric oxide generation are host-protective mechanisms in zebrafish during *Mm* infection[33,37,38]. This makes the zebrafish embryo model for TB a highly suitable model to investigate a possible role for these mechanisms in the anti-mycobacterial effect of Amiodarone.

Here we show that Amiodarone treatment reduces mycobacterial infection in the zebrafish host, in the absence of any direct anti-mycobacterial effect of Amiodarone on *Mm* at doses used. Our studies into the host-mediated action of Amiodarone showed that Amiodarone treatment increased RNS production in our model but did not provide evidence for a major role for the RNS pathway in the anti-mycobacterial effect. Furthermore, while we did observe increased autophagy activity, we did not observe increased targeting of autophagosomes to mycobacteria. We performed transcriptome profiling to identify other pathways that could underly the reduction of bacterial burden after Amiodarone treatment, which revealed major effects of Amiodarone on lysosomal processes. We confirmed these findings by demonstrating that Amiodarone treatment increased levels of lysosomal acidification. These results suggest that Amiodarone treatment has a beneficial effect on defence against mycobacterial infection by modulating functions of lysosomes that contribute to host defence mechanisms, potentially in combination with modulation of autophagy. In conclusion, our results provide the first evidence that Amiodarone, an FDA-approved drug for treating arrhythmias, modulates innate host defence processes that restrict mycobacterial infection in an *in vivo* TB model. We therefore propose Amiodarone as a promising candidate drug to be further tested as HDT against TB.

Results

Amiodarone restricts *Mm* infection in a host-directed manner

A small scale screen of autophagy modulating FDA-approved compounds in the zebrafish embryo model for TB identified Amiodarone as a potential HDT that reduced *Mm* bacterial burden at a dosage of 5 μM (chapter 3). To further determine the optimal dose range, we infected zebrafish embryos with *Mm* at 1 day post fertilisation (dpf) and treated the infected embryos starting at 1 hour post infection (hpi) with vehicle control treatment (DMSO) or with increasing doses (5, 10 and 20 μM) of Amiodarone. Four days post infection (dpi) we assessed bacterial burden by quantifying fluorescent bacterial signal. Amiodarone was able to reduce bacterial burden compared to control treatment in a dose-dependent manner for the 5 and 10 μM groups. However, we observed developmental toxicity such as oedema and lethality in the group treated with 20 μM Amiodarone (Figure 1A-B).

Next, we looked into infection dynamics during Amiodarone treatment to better understand the effect of Amiodarone on *Mm* infection. We infected and treated embryos with Amiodarone (5 and 10 μM) or control treatment as described above. Subsequently, we imaged the embryos daily from 1-4 dpi, which allowed us to compare the development of the infection burden after control or Amiodarone treatment. As early as 2 dpi, a reduction in the Amiodarone-treated groups compared to control could be observed, though we also found developmental toxicity (e.g. oedema and lethality) in the 10 μM group from 3 dpi onward. In all treatment conditions, we observed an increase in bacterial burden. However, at the end point of the experiment Amiodarone treatment with 5 μM reduced the infection burden almost 2-fold compared to control

treatment (Figure 1C). Therefore, Amiodarone does not fully inhibit bacterial growth but does limit the infection burden.

We then wanted to assess whether Amiodarone had a direct effect on *Mm* bacterial growth or survival, as opposed to limiting bacterial burden via a host-directed effect. We thus exposed *Mm* liquid cultures to increasing doses of Amiodarone and measured optical density (OD) to assess bacterial replication at 4 different timepoints (Figure 1D). We found a growth limiting effect of Amiodarone in the *Mm* cultures exposed to 10 µM of Amiodarone, but not in the cultures exposed to 5 µM Amiodarone. These results show that while Amiodarone can have a direct effect on *Mm* growth in liquid cultures, the reduction of bacterial burden we observed in zebrafish embryos treated with 5 µM of Amiodarone can be attributed to host-dependent factors.

To exclude that the host-dependent effect of Amiodarone was associated with major alterations in leukocyte behaviour that might lower its potential application as an HDT, we determined if leukocyte migration was affected. To this end we used an established injury-based migration assay, the tail amputation assay[39,40], in a double transgenic neutrophil and macrophage marker line and assessed the number of neutrophils and macrophages that migrated to the wound-induced site of inflammation (Figure 1E). We did not find significant differences in the numbers of neutrophils and macrophages that accumulated at the site of inflammation after control or Amiodarone (5 µM) treatment (Figure 1F-G).

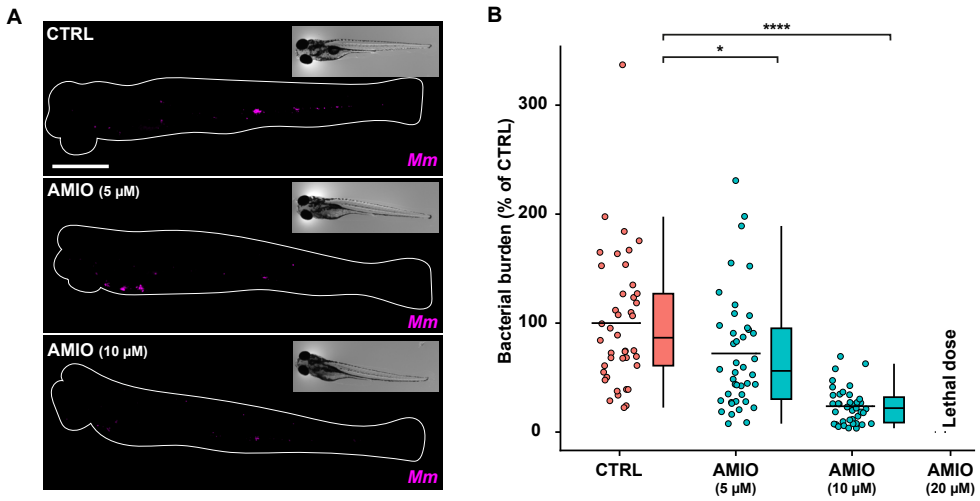

Figure 1. Amiodarone restricts *Mm* infection in a host-directed manner

A. Bacterial burden assay of mWasabi-expressing *Mm*-infected zebrafish larvae treated with increasing doses of Amiodarone (2.5, 5 and 10 µM) or control (DMSO at 0.1% v/v). Treatment was started at 1 hpi and larvae anesthetized at 4dpi for imaging. Representative stereo fluorescent images of whole larvae infected with mWasabi-expressing *Mm*. Magenta shows *Mm*. Scale bar annotates 1 mm.

B. Quantification of bacterial burden shown in A. Bacterial burden was normalized to mean of the control, set at 100% and indicated with the dotted line. Data of 2 experimental repeats were combined (n = 39-42 per group). Each dot represents a single larva. Boxplots with 95% confidence intervals are shown and the black line in the boxplots indicates the group median, while the black line in the dot plot indicates the group mean. Statistical analysis was performed using a Kruskal-Wallis with Dunn's multiple comparisons test.

Figure and figure legend continued on next page.

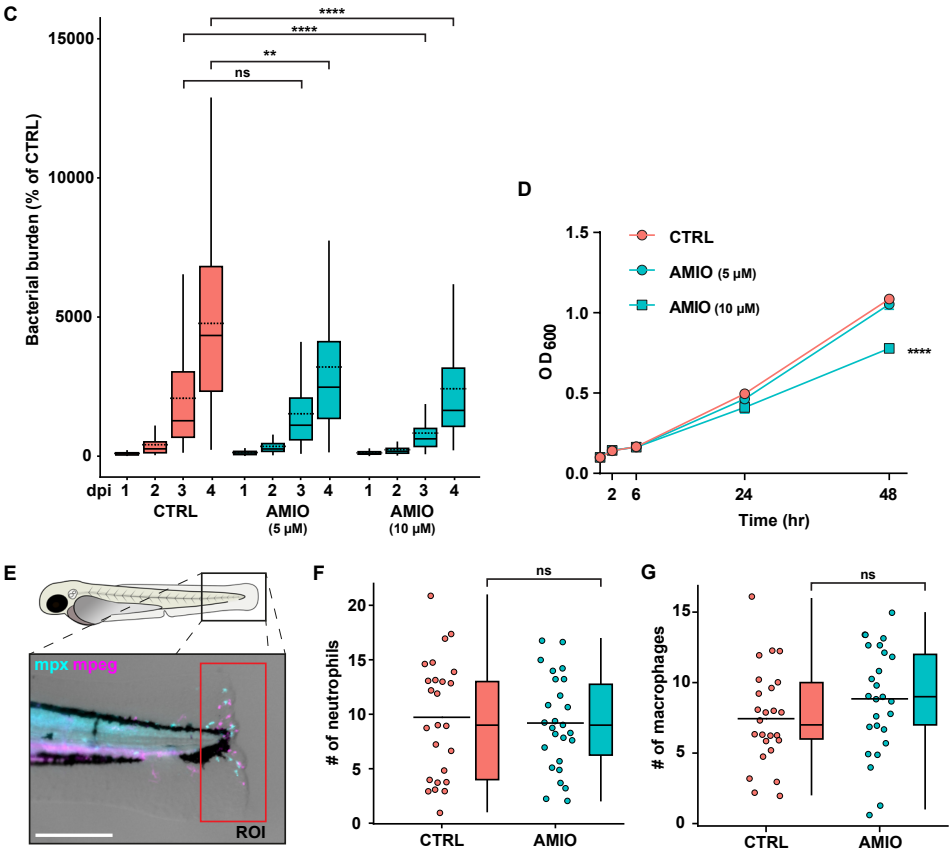

Figure 1. (continued)

C. Bacterial burden assay of mWasabi-expressing *Mm*-infected zebrafish larvae treated with 5 and 10 µM of Amiodarone or control (DMSO at 0.1% v/v). Treatment was started at 1 hpi and larvae were anesthetized at 1, 2, 3 and 4 dpi for imaging. Bacterial burden was normalized to the control (DMSO at 1dpi) and data of 2 experimental repeats were combined (n = 65-70 per group). All larvae in the 10 µM group died between 3-4 dpi. Boxplots with 95% confidence intervals are shown and the black line in the boxplots indicates the group median, while the dotted line indicates the group mean. Statistical analysis was performed between treatment groups per timepoint using a Kruskal-Wallis with Dunn's multiple comparisons test.

D. *Mm* growth in liquid culture during treatment with 5 or 10 µM of Amiodarone or control (DMSO at equal v/v) up to assay endpoint, day 2. Lines depict mean ± standard deviation of 2 experiments. Statistical significance of treatment versus control treatment was tested using a two-way ANOVA with Dunnett's multiple comparisons test.

E. Leukocyte migration assay of mpeg1:mcherryF/mpx:GFP double transgenic zebrafish larvae treated with 5 µM of Amiodarone or control (DMSO at equal v/v). Treatment was started at 1 dpf and larvae were anesthetized and leukocyte migration was induced by tail amputation at 3 dpf. Representative stereo fluorescence images of leukocyte migration towards the injury (4 hours post amputation) are shown. Cyan shows neutrophils (*mpx*:GFP) and magenta shows macrophages (*mpeg1*:mCherryF). The region of interest (ROI) indicates the area for quantification of leukocyte migration. Scale bar annotates 220 µm.

F-G. Quantification of E, showing the number of migrated neutrophils (F) or macrophages (G). Each dot represents a single larva. Boxplots with 95% confidence intervals are shown and the black line in the boxplots indicates the group median, while the black line in the dot plot indicates the group mean. Statistical analysis was performed using a Mann-Whitney test.
(* = p<0.05, ** = p<0.01, *** = p<0.001 and **** = p<0.0001).

We conclude that treatment with 5 µM Amiodarone results in reduction of bacterial burden via a host-directed effect, without apparent adverse effects on the host such as developmental toxicity or altered leukocyte migration. We therefore continued investigating the mechanism by which Amiodarone exerts its anti-mycobacterial effect.

Amiodarone increases RNS activity but not co-localisation of RNS with *Mm* clusters

We considered the possibility that the anti-mycobacterial effect of Amiodarone might be due to its ability to stimulate nitric oxide release[19]. Reactive nitrogen species (RNS), derived from nitric oxide, as well as reactive oxygen species (ROS), are well known anti-microbial molecules[27,41]. Thus, we hypothesized that induction of RNS could be the mechanism via which Amiodarone aids host-resistance to *Mm* in our model. To assess the presence and activity of RNS, we performed immunostaining with an antibody against nitrosylated tyrosine residues (α-nitrotyrosine) that has previously been used in the zebrafish embryo model for TB[33,42]. We first investigated if induction of RNS occurred in uninfected conditions after control treatment or Amiodarone treatment. For this, we used a double fluorescent marker line (*mpx*:GFP/*mpeg*:mCherry) to distinguish neutrophils and macrophages using confocal microscopy in the CHT (Figure 2A). We found an increase in α-nitrotyrosine signal in Amiodarone treated embryos (Figure 2B). Notably, the increase was only observed in neutrophils and not in macrophages without infection, consistent with previous results that demonstrated RNS to be mainly produced by neutrophils during *Mm* infection[33].

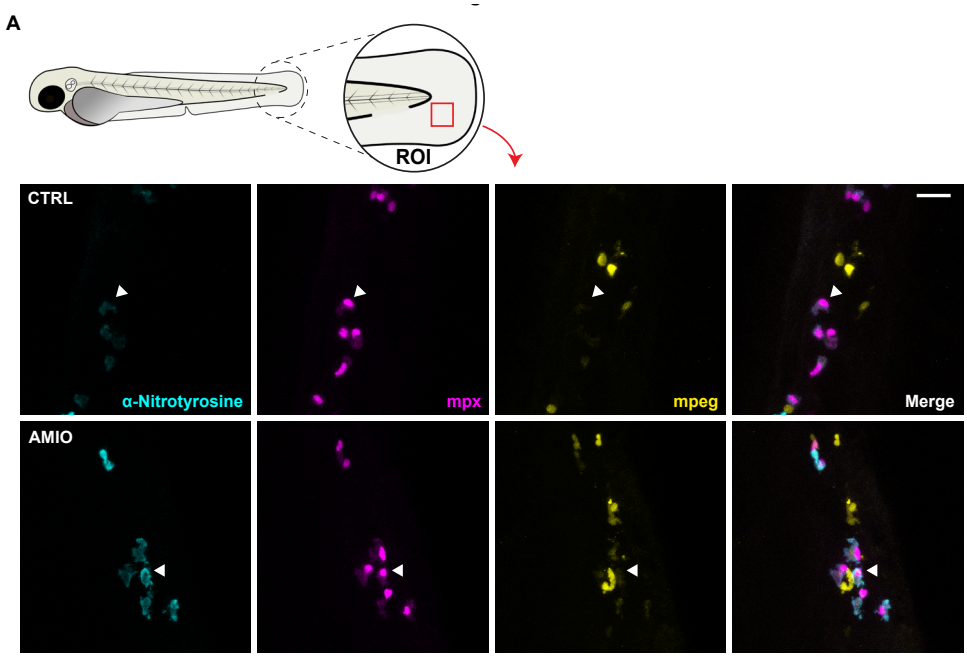

Figure 2. Amiodarone increases RNS levels in neutrophils but not macrophages in absence of infection

A. Confocal microscopy max projection of immunostaining assay using α-nitrotyrosine of mpeg1:mcherryF/mpx:GFP double transgenic zebrafish larvae treated with 5 µM of Amiodarone or control (DMSO et equal v/v). Treatment was started at 1 hpi and at 2 dpi larvae were fixed using 4% paraformaldehyde for imaging. Representative max projection images of the ROI in the tail fin. Cyan shows α-nitrotyrosine signal, magenta shows neutrophils (*mpx*:GFP) and yellow shows macrophages (*mpeg1*:mCherryF). White arrowheads indicate neutrophils showing α-nitrotyrosine signal, indicating RNS production. Scale bar annotates 20 µm.

Figure and figure legend continued on next page.

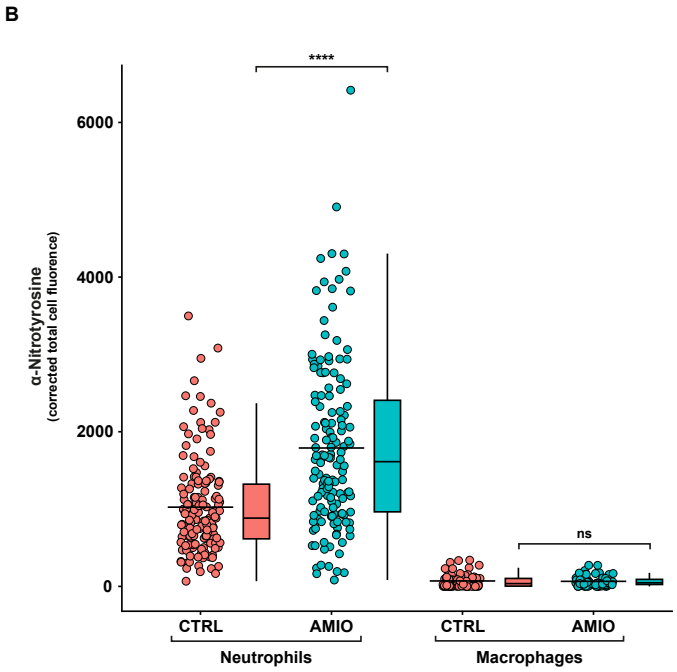

Figure 2. (continued)
B. Quantification of the corrected total cell fluorescence of α-nitrotyrosine signal shown in A per neutrophil or macrophage respectively. Data of 2 experimental repeats were combined. Each data point represents a single cell (n = 147-148 for neutrophils and n = 74 for macrophages). Error bars indicate SEM. Statistical analysis was performed using using a Mann-Whitney test (**** = p<0.0001).

While Amiodarone treatment without infection increased RNS levels in neutrophils, *Mm* infection is mostly constricted to macrophages in the zebrafish model. Therefore, we asked if Amiodarone treatment could boost RNS levels in *Mm*-infected macrophages. To this end, we infected embryos with fluorescently labelled macrophages (*mpeg:*GFP) locally in the tail fin with labelled *Mm* bacteria. We again performed immunostaining with the α-nitrotyrosine antibody and used confocal laser scanning microscopy at 1 dpi to assess RNS activation in the presence of bacteria. As shown by representative images, we were able to detect *Mm*-infected macrophages that were α-nitrotyrosine-positive, but the majority of the α-nitrotyrosine signal was observed outside macrophages (Figure 3A). The total level of α-nitrotyrosine signal inside and outside of macrophages was increased in the Amiodarone treated group compared to control treatment, similar to non-infected conditions (Figure 3B). We then looked specifically at the α-nitrotyrosine signal inside infected macrophages and found it to be significantly increased in the Amiodarone treated group (Figure 3C). In conclusion, macrophages contribute to the increased production of RNS after treatment with Amiodarone in infected conditions, despite that the vast majority of RNS production occurs in neutrophils.

As Amiodarone is able to increase RNS production in infected macrophages as well as in bystander neutrophils, we hypothesized that this increase could be the mechanism underlying the host-protective effect of Amiodarone against *Mm* infection. To address this question, we asked if the increased RNS production was localized around *Mm* clusters. Thus, we analysed colocalization between α-nitrotyrosine signal and *Mm* clusters and macrophages. Because 2D maximum projection images of confocal

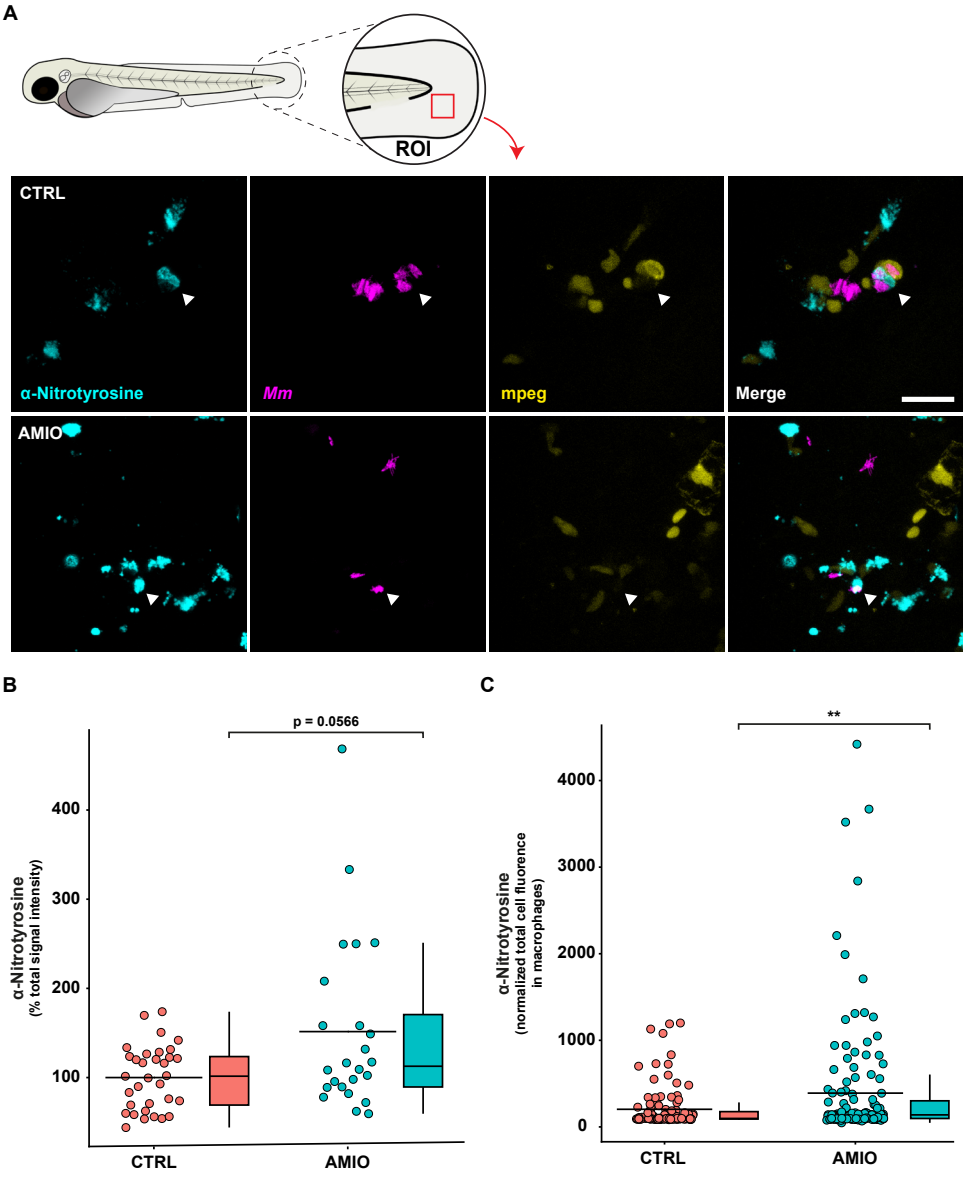

Figure 3. Amiodarone increases total and macrophage specific RNS levels in the presence of infection

A. Confocal microscopy max projection of immunostaining assay using α-nitrotyrosine of mCherryexpressing *Mm*-infected mpeg1:GFP transgenic zebrafish larvae treated with 5 μM of Amiodarone or control (DMSO et equal v/v). Treatment was started at 1 hpi and at 2 dpi larvae were fixed using 4% paraformaldehyde for imaging. Representative max projection images of the ROI in the tail fin. Cyan shows α-nitrotyrosine signal, magenta shows *Mm* and yellow shows macrophages (*mpeg1*:GFP). White arrowheads indicate interactions between *Mm* and the innate immune system. Scale bar annotates 20 μm.

B. Quantification of the total α-nitrotyrosine signal intensity shown in A. Data of 3 experimental repeats were combined. Each data point represents a single embryo (n = 24-33). Error bars indicate SEM. Statistical analysis was performed using a Mann-Whitney test.

C. Quantification of the normalized total cell fluorescence in macrophages shown in A. Data of 2 experimental repeats were combined. Each data point represents a single cell (n = 111-135). Error bars indicate SEM. Statistical analysis was performed using a Mann-Whitney test.
(** = p<0.01).

microscopy data potentially misrepresents colocalization in the Z-dimension, we used Imaris image analysis software to construct 3D images from the Z-stacks obtained in the tail fin infection experiment with confocal microscopy (Figure 4A). Quantification of the percentage of volume colocalization between macrophages and α-nitrotyrosine signal based on the 3D reconstruction, showed that only ~3.5% of the signal colocalized with macrophages. Furthermore, we found no significant difference between control treatment and Amiodarone treatment (Figure 4B). We then quantified volume colocalization of *Mm* clusters and α-nitrotyrosine signal based on the 3D reconstruction, which also revealed no significant difference between control treatment or Amiodarone-treated embryos (Figure 4C). This suggests that the observed increase in RNS production is not leading to more RNS that is specifically localized at *Mm* clusters, either intra- or extracellular. We then reasoned that limiting the analysis only to direct colocalization could overlook bacterial exposure to RNS at earlier time points that could be relevant for bacterial clearance. Thus, we quantified the number of α-nitrotyrosine spots in the vicinity of non-infected macrophages, *Mm* clusters, or infected macrophages to detect if Amiodarone treatment increased RNS around bacteria, which could explain the lower bacterial burden. We found no significant differences in the total number of α-nitrotyrosine spots between control treatment or Amiodarone treatment groups, nor in a 4 µM radius around *Mm* clusters, in a 2 µM radius around macrophages or in a 2 µM radius around infected macrophages (Figure 4D).

Taken together we conclude that, while Amiodarone induces RNS production in neutrophils and infected macrophages, there is no evidence for a specific increase of RNS at or around *Mm* clusters, either within macrophages or in the nearby extracellular environment.

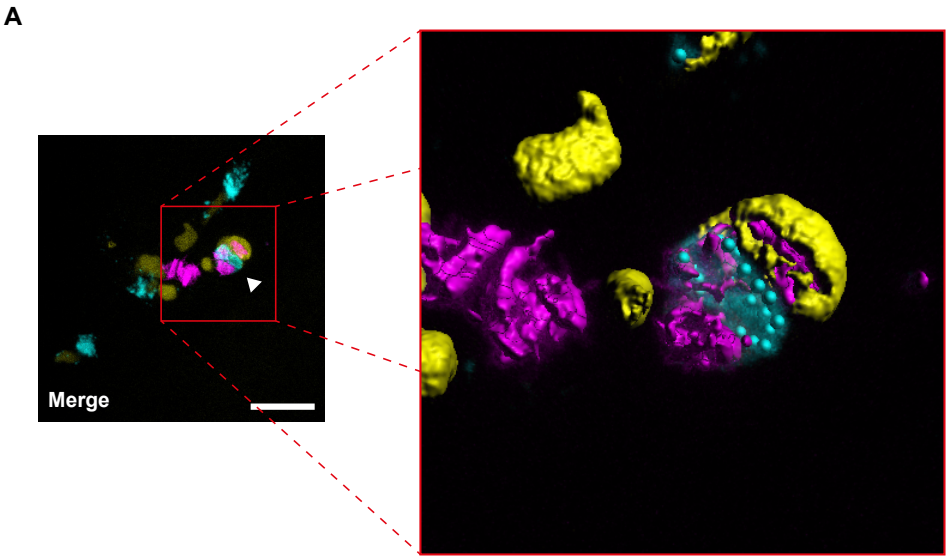

Figure 4. Amiodarone does not increase colocalization of α-nitrotyrosine signal with macrophages nor *Mm*
A. 3D rendering of confocal image shown in figure 3A made with Imaris. Cyan shows α-nitrotyrosine signal, magenta shows *Mm* and yellow shows macrophages (*mpeg1*:GFP). White arrowhead indicates interactions between *Mm* and the innate immune system. The 3D rendering was made based on the image data with Imaris software.

Figure and figure legend continued on next page.

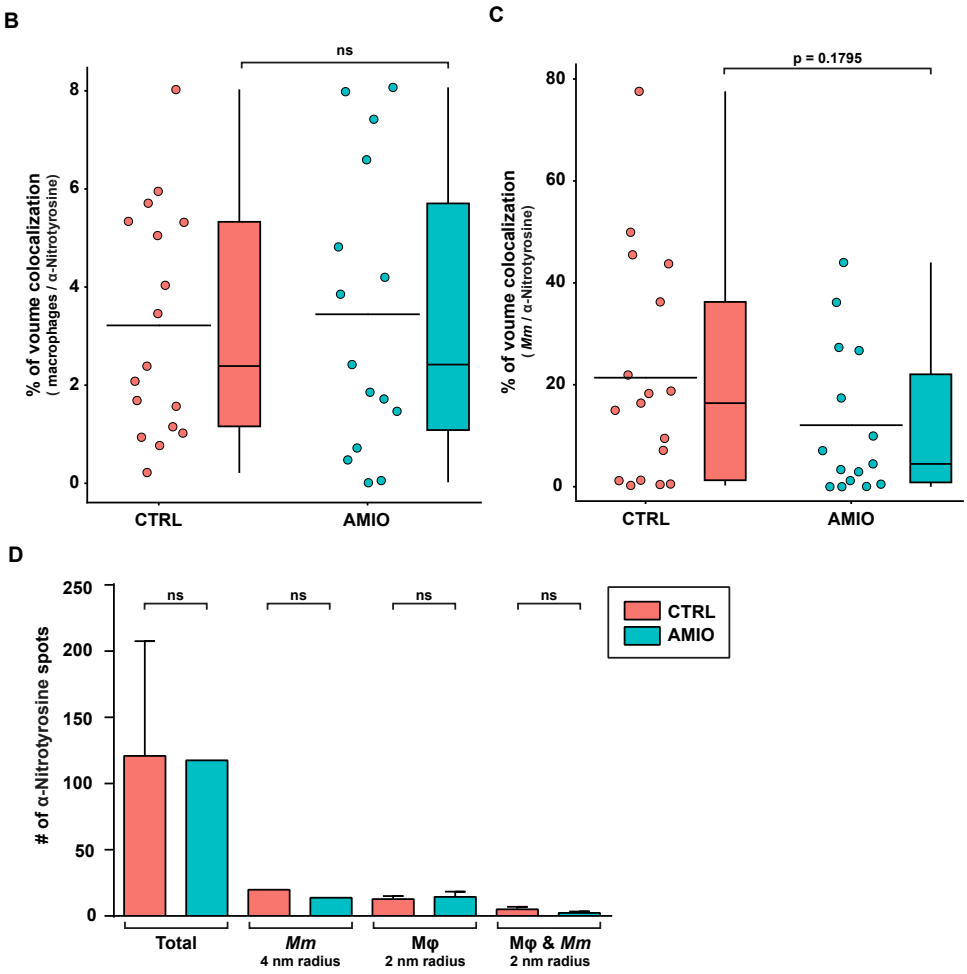

Figure 4. (continued)

B. Quantification of the colocalization of macrophage and α-nitrotyrosine signal based on volume calculated using the 3D rendering in Imaris shown in A. Data of 2 experiments were combined. Each data point represents a single embryo (n = 15-17). Error bars indicate SEM. Statistical analysis was performed using a Mann-Whitney test.

C. Quantification of the colocalization of *Mm* and α-nitrotyrosine signal based on volume calculated using the 3D rendering in Imaris shown in A. Data of 2 experiments were combined. Each data point represents a single embryo (n = 15-17). Error bars indicate SEM. Statistical analysis was performed using a Mann-Whitney test.

D. Quantification of α-nitrotyrosine signal spots in the proximity of *Mm* clusters, macrophages, or infected macrophages using the 3D rendering in Imaris shown in A. Data of 2 experiments were combined (n = 15-17 embryos in total). Error bars indicate SEM. Statistical analysis for each proximity quantification was performed separately using a Kruskal-Wallis with Dunn's multiple comparisons test.

Amiodarone restricts *Mm* bacterial burden independent of RNS production

Because of the known host protective role of RNS[20,27,28,43] and the fact that we did not observe a localized increase in RNS production around *Mm* clusters after Amiodarone treatment, we asked if Amiodarone treatment would still reduce bacterial burden if RNS production was inhibited. Therefore, we used chemical inhibition of NOS enzymes that produce RNS. We used a specific iNOS inhibitor (L-NIL) or a pan-NOS inhibitor (L-NAME) to block NOS activity. We hypothesized that inhibiting iNOS and NOS activity would abolish the effect of Amiodarone treatment on bacterial burden if increased RNS production is indeed the mechanism by which Amiodarone exerts its lowering effect on bacterial burden. Thus, we infected zebrafish embryos at 1 dpf and treated with control treatment or Amiodarone in presence or absence of L-NIL. Treatment of infected embryos with Amiodarone resulted in reduced bacterial burden compared to control treatment with or without iNOS inhibition (Figure 5A). Similarly, when infected zebrafish

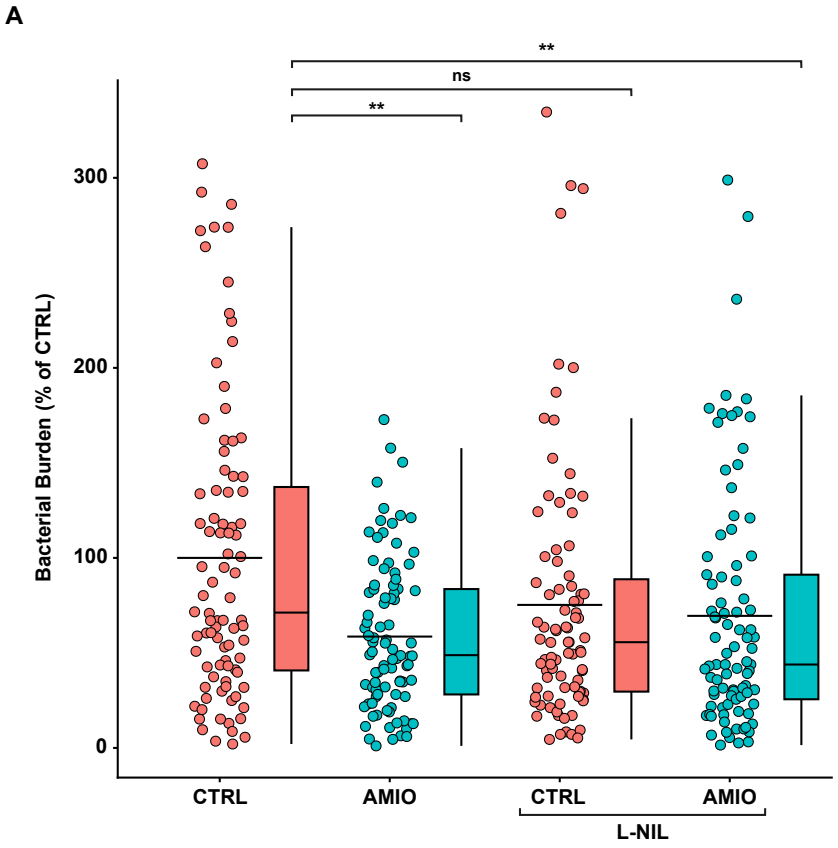

Figure 5. Amiodarone restricts *Mm* bacterial burden independent of RNS production

A. Bacterial burden assay of mWasabi-expressing *Mm*-infected zebrafish larvae treated with 5 µM of Amiodarone, 200 µM of the specific iNOS inhibitor L-NIL, a combination of 5 µM Amiodarone and 200 µM L-NIL or control (DMSO at 0.25% v/v). Treatment was started at 1 hpi and larvae anesthetized at 4dpi for imaging. Bacterial burden was normalized to mean of the control, set at 100% and indicated with the dotted line. Data of 3 experimental repeats were combined (n = 88-90 per group). Each dot represents a single larva. Boxplots with 95% confidence intervals are shown and the black line in the boxplots indicates the group median, while the black line in the dot plot indicates the group mean. Statistical analysis was performed using a Kruskal-Wallis with Dunn's multiple comparisons test.

Figure and figure legend continued on next page.

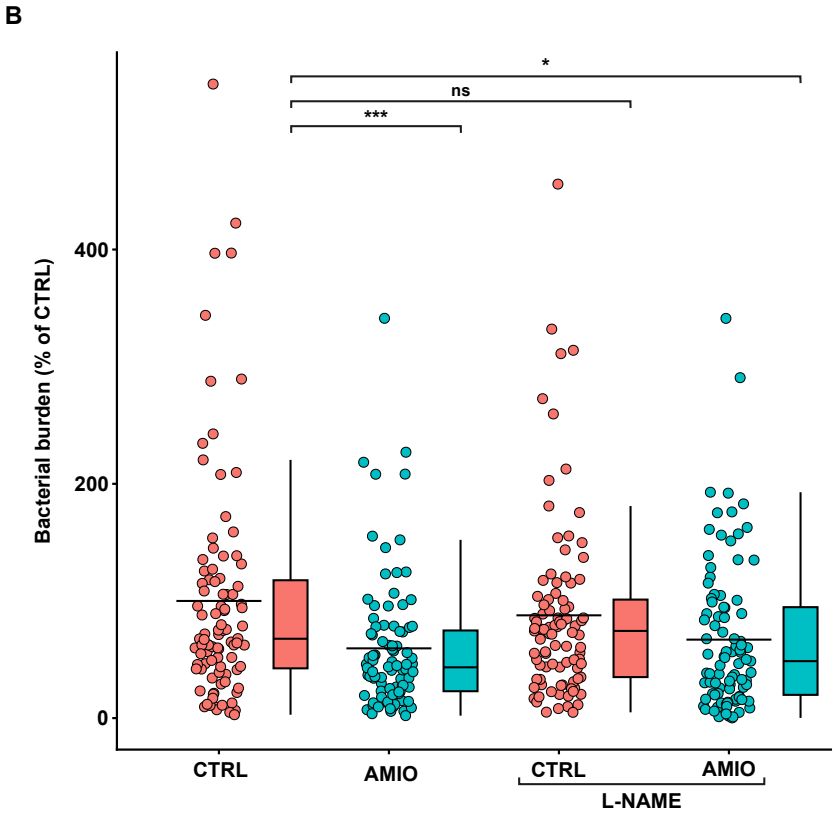

Figure 5. (continued)

B. Bacterial burden assay of mWasabi-expressing *Mm*-infected zebrafish larvae treated with 5 µM of Amiodarone, 200 µM of the pan-NOS inhibitor L-NAME, a combination of 5 µM Amiodarone and 200 µM L-NAME or control (DMSO at 0.45% v/v). Treatment was started at 1 hpi and larvae anesthetized at 4dpi for imaging. Bacterial burden was normalized to mean of the control, set at 100% and indicated with the dotted line. Data of 3 experimental repeats were combined (n = 92-94 per group). Each dot represents a single larva. Boxplots with 95% confidence intervals are shown and the black line in the boxplots indicates the group median, while the black line in the dot plot indicates the group mean. Statistical analysis was performed using a Kruskal-Wallis with Dunn's multiple comparisons test.
(* = p<0.05, ** = p<0.01 and *** = p<0.001).

embryos were treated with control treatment or Amiodarone in presence or absence of L-NAME, the effectivity of Amiodarone treatment was not affected and reduced bacterial burden compared to control treatment was observed regardless of pan-NOS inhibition (Figure 5B). This suggests that, while Amiodarone treatment leads to an increase in RNS production, the effect of Amiodarone on reduction of bacterial burden is independent of RNS production and is mediated via different host pathways.

Amiodarone induces an increase in autophagosomes but not in autophagic targeting of *Mm* clusters

Next, we investigated if the anti-mycobacterial effect of Amiodarone could be due to the autophagy-inducing activity that has been reported for this compound[13,15]. We first looked into autophagic activity in uninfected zebrafish embryos using a fluorescent reporter line for the autophagy marker Lc3[44]. We treated 3 dpf embryos for 24 hours with Amiodarone or control treatment and imaged the tail fin using confocal laser scanning

microscopy[45]. We quantified GFP-Lc3 positive structures and observed a significant increase in the number of GFP-Lc3 structures in the Amiodarone treated group (Figure 6A-B) compared to control treatment. Therefore, we conclude that Amiodarone results in an increased number of autophagic vesicles under uninfected conditions.

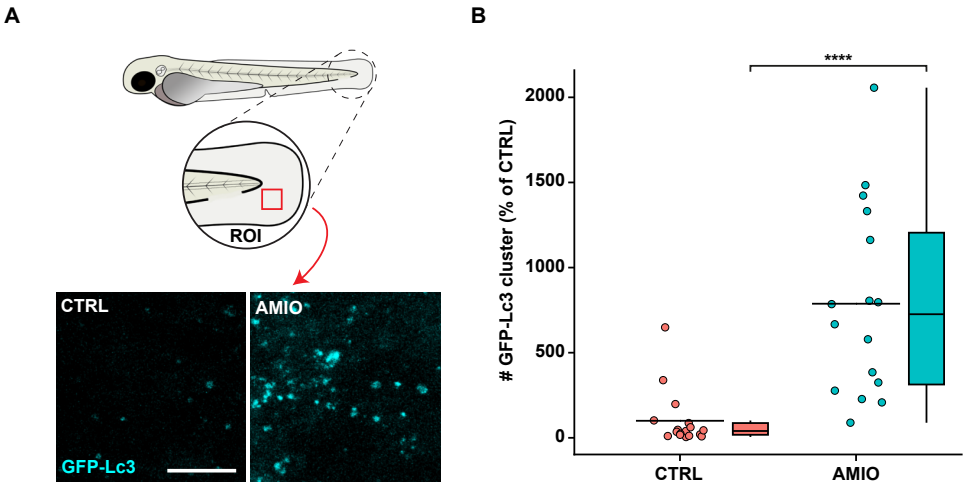

Figure 6. Amiodarone induces an increase in autophagosomes

A. Confocal microscopy max projection of transgenic GFP-Lc3 zebrafish larvae treated with 5 µM of Amiodarone or control (DMSO at equal v/v). Treatment was started at 3 dpf and larvae were fixed with 4% paraformaldehyde at 4 dpf for imaging. Representative max projection images of GFP-Lc3 positive vesicles in the indicated region of imaging (ROI) in the tail fin are shown. Cyan shows GFP-Lc3 positive vesicles. Scale bar annotates 10 µm.

B. Quantification of GFP-Lc3 structures shown in A. Data were normalized to the control and data of 2 experimental repeats were combined (n = 16-17 per group). Each dot represents a single larva. Boxplots with 95% confidence intervals are shown and the black line in the boxplots indicates the group median, while the black line in the dot plot indicates the group mean. Statistical analysis was performed using a Mann Whitney test.
(**** = p<0.0001).

Because we observed an increase in autophagic vesicles after Amiodarone treatment, we next investigated *Mm* clearance via the autophagolysosomal pathway after Amiodarone treatment. We therefore assessed co-localisation between GFP-Lc3 and *Mm* clusters by infecting 1 dpf embryos of the GFP-Lc3 reporter line and imaged the embryos at 2 dpi in the caudal hematopoietic tissue (CHT) region using confocal microscopy. We selected the CHT because it is a region where infected macrophages are known to aggregate, which is the first step in granuloma formation[36]. In both control treatment and Amiodarone treatment groups, we observed bacterial clusters that are decorated by GFP-Lc3 and bacterial clusters that are GFP-Lc3 negative (Figure 7A-B). Besides treatment with control treatment or Amiodarone, we also used the V-ATPase inhibitor bafilomycin (Bafilomycin A1, 160nM) to prevent lysosomal acidification and block autophagic flux, allowing to distinguish between effects of Amiodarone on autophagic targeting of *Mm* from effects on *Mm* degradation through the autophagolysosomal pathway. As expected, blocking flux with bafilomycin resulted in an overall increase of GFP-Lc3 signal in both control treatment and Amiodarone treatment conditions (Figure 7D-G). However, we did not observe a difference in the percentage of *Mm* clusters

positive for GFP-Lc3 structure(s) between control treatment or Amiodarone treatment in absence or presence of bafilomycin (Figure 7G). Thus, blocking autophagic flux did not reveal an increase in *Mm*-containing autophagomes due to Amiodarone treatment.

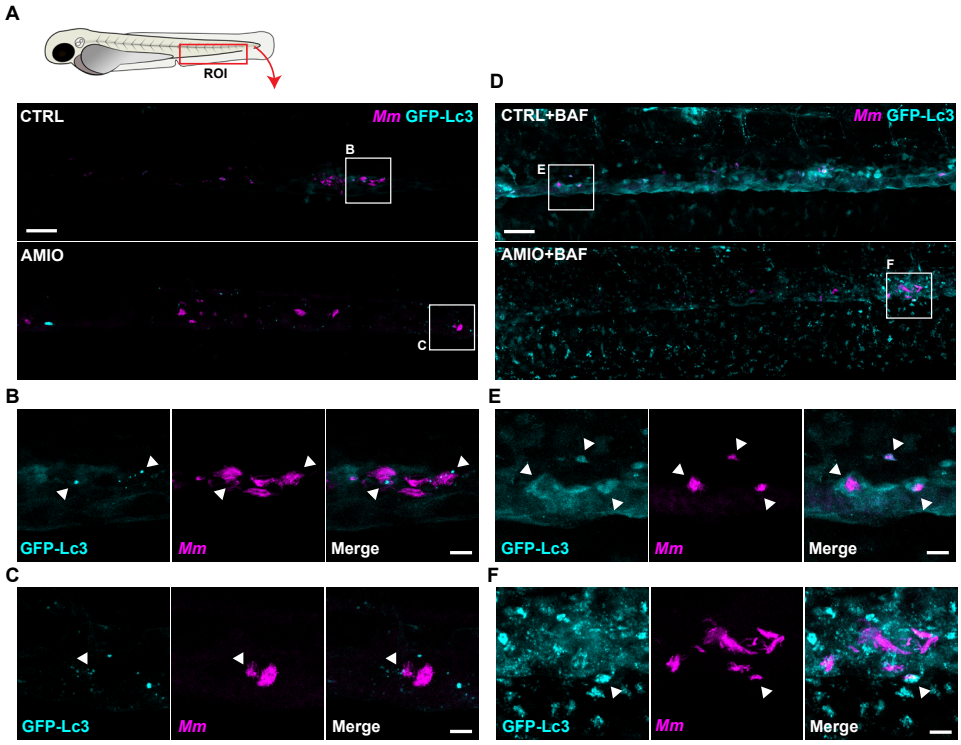

Figure 7. Amiodarone does not induce an increase in autophagic targeting of *Mm* clusters

A. Confocal microscopy max projection of mCherry-expressing *Mm*-infected transgenic GFP-Lc3 zebrafish larvae treated with 5 µM of Amiodarone or control (DMSO at equal v/v). Treatment was started at 1 hpi and at 2 dpi larvae were fixed with 4% paraformaldehyde for imaging. Representative max projection images of the ROI in the caudal hematopoietic tissue (CHT) region are shown. Cyan shows GFP-Lc3 positive vesicles and magenta shows *Mm*. Scale bar annotates 50 µm.

B-C. Enlargement of areas indicated in A. Cyan shows GFP-Lc3 positive vesicles and magenta shows *Mm*. Arrowheads indicate GFP-Lc3-positive *Mm* clusters. Scale bar annotates 10 µm.

D. Confocal microscopy max projection of mCherry-expressing *Mm*-infected transgenic GFP-Lc3 zebrafish larvae treated with 5 µM of Amiodarone and 160 nm of bafilomycin or control (DMSO at equal v/v). Treatment was started at 1 hpi and at 2 dpi larvae were fixed with 4% paraformaldehyde for imaging. Representative max projection images of the ROI in the caudal hematopoietic tissue (CHT) region are shown. Cyan shows GFP-Lc3 positive vesicles and magenta shows *Mm*. Scale bar annotates 50 µm.

E-F. Enlargement of areas indicated in D. Cyan shows GFP-Lc3 positive vesicles and magenta shows *Mm*. Arrowheads indicate GFP-Lc3-positive *Mm* clusters. Scale bar annotates 10 µm.

Figure and figure legend continued on next page.

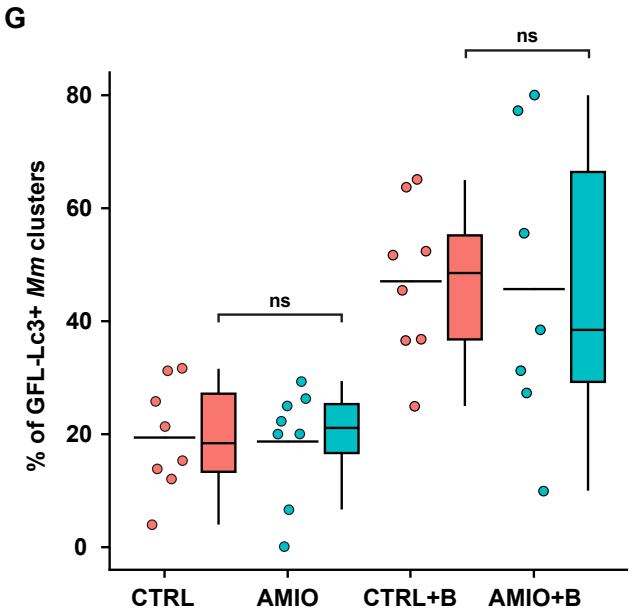

Figure 7. (continued)
G. Quantification of GFP-Lc3 positive *Mm* clusters in the CHT region shown in A and D normalized to the control (n = 8 per group). Each dot represents a single larva. Boxplots with 95% confidence intervals are shown and the black line in the boxplots indicates the group median, while the black line in the dot plot indicates the group mean. Statistical analysis was performed using a Kruskal-Wallis with Dunn's multiple comparisons test.

Amiodarone increases lysosomal staining

Considering that Amiodarone has also been reported to affect the endocytic pathway[18], we performed LysoTracker staining to detect acidified intracellular compartments. We treated uninfected embryos with control treatment or Amiodarone (5 µM) starting at 30 hpf for 2 days. At 3 dpf we performed LysoTracker staining and imaged the tail fin of the embryos using confocal microscopy. We observed a clear increase in LysoTracker signal in the embryos treated with Amiodarone (Figure 8A-B). Moreover, the LysoTracker positive vesicles were significantly enlarged (300%) compared to those in control treatment treated embryos (Figure 8C). The increase in both the number of positive vesicles combined with the increase in vesicle size in these embryos may provide an explanation for the antimycobacterial effect of Amiodarone.

RNA sequencing confirms major effects on lysosomal function *in vivo*

Finally, we performed RNA sequencing analysis to investigate the transcriptional effects of Amiodarone treatment and get more insight into the cellular pathways that are affected by Amiodarone treatment. The RNA sequencing analysis of Amiodarone was performed in conjuncture with RNA sequencing analysis of Tamoxifen, another potential HDT that was shown to be effective against *Mm* in zebrafish (chapter 4). For both Amiodarone and Tamoxifen, the same control treatment-treatment groups and analysis methods were used. When analysing the transcriptome of the control treatment treated larvae, we found consistent results with earlier transcriptomic data of *Mm* infected zebrafish, showing upregulation of genes associated with inflammation and host defence as is described in chapter 4[46]. Amiodarone treatment of non-infected larvae caused differential expression of 381 genes, including genes involved in autophagy and

lysosomal processes, such as *p62* (*sqstm1*) and *lamp1a* (Supplementary Data File 1).

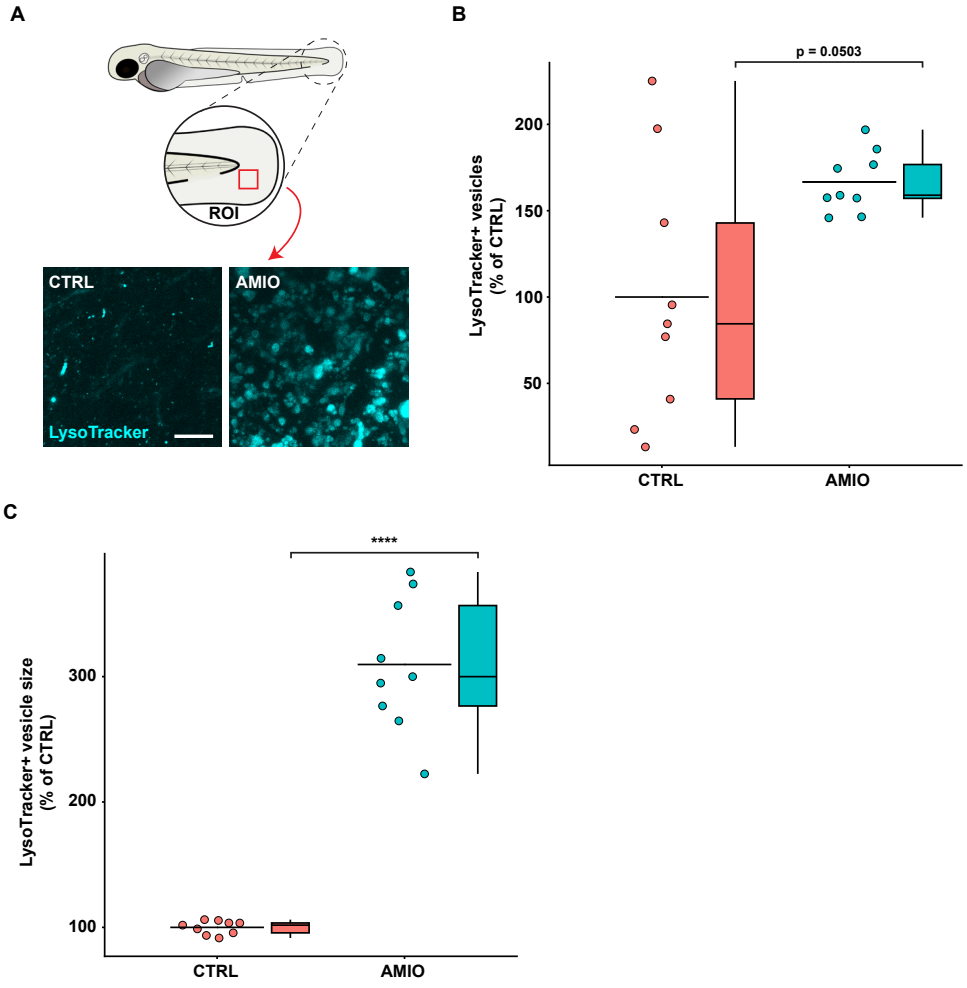

Figure 8. Amiodarone induces lysosomal activity

A. Confocal microscopy max projection of the indicated ROI in zebrafish larvae treated with 5 µM of Amiodarone or control (DMSO at equal v/v). Treatment was started at 31 hpf and at 3 dpf larvae were immersed in 5 µM of LysoTracker Red DND-99 for 1 hour and subsequently anesthetized for imaging. Cyan shows acidic vesicles. Scale bar annotates 10 µm.

B. Quantification of LysoTracker-positive vesicles shown in A normalized to the control and data of 2 experimental repeats were combined (n = 9 per group). Each dot represents a single larva. Boxplots with 95% confidence intervals are shown and the black line in the boxplots indicates the group median, while the black line in the dot plot indicates the group mean. Statistical analysis was performed using a Mann Whitney test.

C. Quantification of the size of LysoTracker-positive vesicles shown in A normalized to the control and data of 2 experimental repeats were combined (n = 9 per group). Each dot represents a single larva. Boxplots with 95% confidence intervals are shown and the black line in the boxplots indicates the group median, while the black line in the dot plot indicates the group mean. Statistical analysis was performed using a Mann Whitney test.
(****p=<.0001).

We proceeded to analyse which genes were differentially regulated in control treatment larvae by both of the two applied stimuli: Amiodarone treatment and infection. We found 10 genes whose expression was upregulated by both stimuli, independent of each other (Figure 9A-B, Supplementary Table S1). One of these genes is cathepsin C (*ctsc*), which is central in the lysosomal pathway in immune cells. Furthermore, some other genes we found to be upregulated are related to immune processes (*c4b*, *cfb*, *ncf1*, *cp*, *stat3*), suggesting Amiodarone treatment in absence of infection is able to modulate and perhaps prime the immune system. We then looked at the interaction between Amiodarone treatment and infection. We found 17 genes whose expression level was altered by Amiodarone treatment during infection (Figure 9C, Supplementary Table S2). Interestingly, we again found upregulation of immune related genes (*cfb* and *ncf1*) which are components of the complement and phagocyte NADPH oxidase systems. This result could suggest Amiodarone activates these innate immune defence mechanisms. Together with iNOS, the NADPH oxidase mediates RNS production. Notably, the upregulation of *ncf1* is in line with the observed effect of Amiodarone on increased RNS levels.

We then focused on the broad systemic effects of Amiodarone treatment and looked at the differences in the transcriptome of uninfected larvae after control treatment and Amiodarone treatment. This analysis revealed prominent differences in the expression of genes in pathways involved in (phago)lysosomal processes. Specifically, pathway enrichment against the KEGG database revealed enrichment of genes from the phagosome and lysosome pathways (Supplementary Table S3). Furthermore, Gene Ontology and GSEA highlighted that genes with molecular functions such as hydrolase activity, biological processes such as lysosomal transport, and genes belonging to the

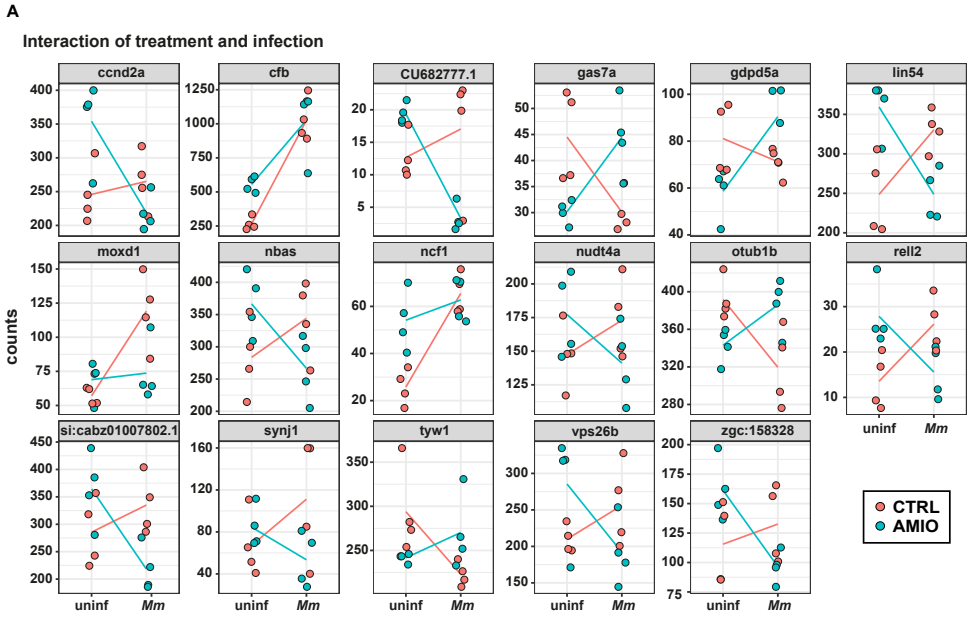

Figure 9. Amiodarone treatment modulates leukocyte gene expression

A. Interaction between Amiodarone treatment and infection in genes that are differentially regulated (s-value ≤ 0.005) and whose expression during infection was found to be dependent on Amiodarone treatment. Each dot represents the normalized gene read count of a single biological replicate (n = 10 larvae), while the line connects the means.

Figure and figure legend continued on next page.

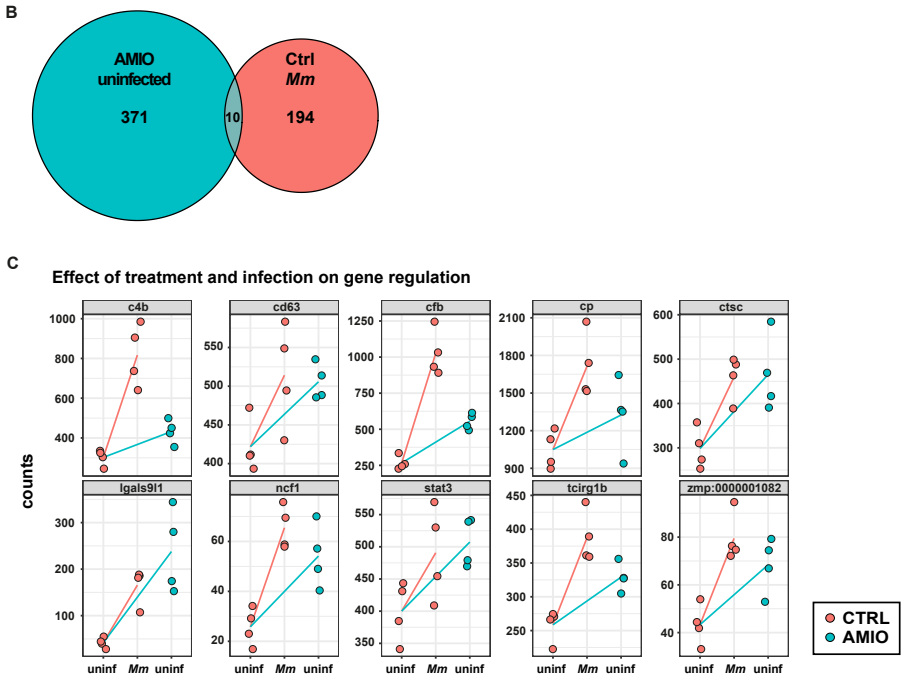

Figure 9. (continued)

B. Venn diagram showing the total number of genes differentially regulated by Amiodarone treatment in the absence of infection and by *Mm* infection in the absence of Amiodarone treatment.

C. Normalized gene read counts of genes whose expression was regulated by both Amiodarone treatment and *Mm* infection individually. Each dot represents the normalized gene read count of a single group of larvae (n = 10), while the line connects the means.

lysosome compartment were enriched in response to Amiodarone treatment. In addition, pathways associated with phototransduction and retinol metabolism were enriched (Supplementary Table S3), a possible reflection of the association of Amiodarone with optic neuropathies[47,48]. Taken together, the upregulation of the (auto)phagolysosomal pathway and the observed increase in numbers and size of lysosomal vesicles lead us to propose that Amiodarone reduces *Mm*-infection burden in a host-dependent manner by increasing (auto)phagolysosomal activity.

Discussion

Amiodarone is widely used as an antiarrhythmic drug that prolongs cardiomyocyte contraction by blocking calcium channels. In addition, via NO release, it causes vasodilation which is also believed to contribute to its cardiovascular protective effect[19,49]. Unrelated to its current therapeutic use, it is known that Amiodarone induces autophagy and affects the endocytic pathway[13,15,18], which are both crucial processes in the intracellular defence against infections with many intracellular pathogens, including *Mtb*[17,50]. In an effort to find new HDTs for TB, we performed a small screen of autophagy modulating compounds (chapter 3). Amiodarone was found to be effective against mycobacterial infection in cultured macrophages and in zebrafish. Here, we investigated the possible mechanisms underlying the anti-mycobacterial effect of

Amiodarone. Importantly, we show that Amiodarone treatment leads to an increase in RNS and (auto)phagolysosomal activity, two important mechanisms in host defence against mycobacterial infection, further substantiating the potential of repurposing Amiodarone as an HDT for TB.

We showed the effect of Amiodarone on RNS and (auto)phagolysosomal activity by utilizing the zebrafish embryo model for TB[34,35,51,52]. This model proved highly suitable for this study for several reasons. Firstly, it has been previously used to study both the RNS and autophagy pathways in relation to mycobacterial infection, showing that both processes contribute to host defence *in vivo*[33,37,38]. Secondly, the model allows us to perform treatments and co-treatments of Amiodarone and chemical inhibitors simultaneously in an easy manner by drug administration to the embryo medium (chapter 3). Thirdly, the model is highly suitable for fluorescent and confocal microscopy using both live and fixated samples[45,53]. This allowed us to visualize and quantify cellular processes in the context of a whole organism. And lastly, transcriptome analysis can be conducted at whole organism level in this model, enabling us to identify host defence pathways enhanced by Amiodarone. Transcriptional regulation by Amiodarone treatment of pathways related to phototransduction and retinol metabolism (Supplementary Tabl S3) are in line with the known clinical side effect of Amiodarone to induce optic neuropathy in humans[47,48], further supporting the translational relevance of the model. While Amiodarone is considered a relatively safe antiarrhythmic drug, it has a number of well-known and sometimes serious side-effects including lung toxicity, liver injury and vision problems. There are several case studies of lung disease associated with Amiodarone treatment[54,55]. Of note to our study, a case has also been reported where side effects of Amiodarone-induced lung injury had masked an underlying TB infection[56]. To the best of our knowledge, Amiodarone has not yet been shown to have anti-TB effects, either as an HDT or directly as an antibiotic.

Our analysis of Amiodarone on *Mm* infection in zebrafish revealed a significant increase in autophagic vesicles that led us to hypothesize that increased autophagy was responsible for the reduction of bacterial burden. The role of autophagy as a defence mechanism against intracellular pathogens, including mycobacterium, is well known[17,21,57]. However, after Amiodarone treatment we did not observe increased colocalization of the autophagy marker GFP-Lc3 with *Mm*-clusters, nor when blocking autophagic flux using bafilomycin during Amiodarone treatment. While these results did not provide evidence for increased autophagy-mediated degradation, LysoTracker analysis showed a massive increase in acidic vesicle size and numbers. Furthermore, transcriptome analysis showed upregulation of the (auto)phagolysosomal pathway. Although further elucidation of the effects of Amiodarone on (auto)phagolysosomal activity is needed, our results are in line with known effects of Amiodarone on the endocytic pathway. It has been previously shown that the accumulation of Amiodarone in endosomes and lysosomes play a role in restricting viral replication in the cases of Ebola and SARS[18]. It has even been proposed that Amiodarone could restrict SARS-CoV2 and is therefore an interesting drug candidate to treat Covid-19[58]. The mechanism by which Amiodarone restricts viral replication, could well be similar to the restriction of mycobacterial infection. For instance, viral replication is slowed after Amiodarone treatment by containing virus particles in endocytic and lysosomal compartments, preventing the release of viral particles in the cytoplasm. Likewise, containing bacteria in these compartments could lead to slower replication and less spread through the host.

The increase in acidic vesicle size and numbers in Amiodarone-treated zebrafish embryos shows parallels with the phenotypes seen in zebrafish models for lysosomal storage disorders, resulting from the accumulation of lipids in lysosomes[59]. Amiodarone is also known to induce phospholipidosis, the accumulation of phospholipids in lysosomal structures[54,60]. The relationship of these conditions with mycobacterial infections

is not well understood. The possibility is proposed, and debated, that heterozygous carriers of mutations underlying lysosomal storage disorders could provide a selective advantage for resistance against TB[61]. It has been shown that the increase in intracellular cargo, contained in lysosomes, has a negative impact on macrophage migration, and macrophage migration is known to play a role in the dissemination of bacteria[62]. Severe lysosomal storage defects have been shown to impair macrophage migration to such extent that macrophage necrosis resulted in exacerbated extracellular bacterial growth[59]. However, we did not observe reduced migration of macrophages after Amiodarone treatment. Still, it is conceivable that infected macrophages migrate less in Amiodarone-treated hosts. In contrast to the severe migration defect associated with lysosomal storage disorders, a moderate reduction of macrophage migration has been shown to have a host-protective effect because this limits spreading of bacteria through the host. Furthermore, macrophages that have reduced migration capability were observed to increase their lysosomal compartment, which augments the microbicidal capacity[63]. Therefore, the Amiodarone-induced increase in the lysosomal compartment, together with a possible reduction of infected-cell migration, could be beneficial for the host combatting intracellular bacterial infection.

In addition to the increased (auto)phagolysomal activity, our results show a marked increase of RNS production by Amiodarone in macrophages and neutrophils measured by α-nitrotyrosine signal. In line with previous observations in the zebrafish model[33], most of the RNS production occurred in neutrophils and independent of infection. We also detected increased RNS production in infected macrophages, but these RNS levels were much lower than in neutrophils despite the fact that macrophages are the main cell type carrying mycobacteria. However, we were unable to link the induction of NO production and subsequent increase in RNS activity directly to the reduction of mycobacterial burden because colocalization did not reveal a specific increase in RNS around mycobacteria in infected cells. Furthermore, we found no evidence that chemical inhibition of iNOS or the use of a pan-NOS inhibitor eliminates the anti-mycobacterial effect of Amiodarone. Together these results indicate that while RNS is increased by Amiodarone, the effect does not play a substantial role in combating mycobacterial infection. A possible explanation for the limited effect of increased RNS levels is that Amiodarone was applied after infection in our study. In agreement, activating RNS defences by stabilizing Hif-1α prior to infection led to lower bacterial burden, while no effect was observed when RNS production was blocked chemically or genetically during the course of infection[33]. Another explanation for the limited role that RNS has in the host defence response to mycobacterial infection could be that mycobacterium is able to counteract the RNS response of the host[32,42]. Based on these data, increased RNS production may contribute to the anti-mycobacterial effect of Amiodarone, but it is likely that additional innate immune effects are responsible for increased resistance of Amiodarone-treated zebrafish embryos to *Mm* infection.

Taken together, we have identified several innate host defence pathways that are enhanced by Amiodarone treatment, but have not fully elucidated the mechanism by which Amiodarone reduces mycobacterial burden. It is possible that the (auto) phagolysosomal pathway is activated by Amiodarone as a general result of cellular stress, caused by disruption of mitochondrial function[64]. In addition, Amiodarone might prime the innate immune system by upregulation of among others the NAPDH oxidase pathway, which potentially cooperates with Amiodarone-inducible nitric oxide signalling. Indeed, we show that treatment with Amiodarone alters the RNS and (auto)phagolysomal pathways, two relevant pathways in cellular defence against mycobacterial infection. Amiodarone treatment results in lower mycobacterial burden and we propose that because of the activation of these pathways, intracellular bacteria are less successful in resisting degradation. This makes Amiodarone a highly interesting compound to further study as a potential HDT against tuberculosis.

Materials and methods

Chemicals

Amiodarone-HCl (Amiodarone) was purchased from Sigma-Aldrich, Zwijndrecht, The Netherlands. L-NAME HCl (L-NAME) and L-NIL Hydrochloride (L-NIL) were purchased from Bio-Connect, Huissen, The Netherlands. All compounds were dissolved in 100% dimethyl sulfoxide (DMSO, Sigma-Aldrich) in stock concentrations of 10 mM, aliquoted and kept at -80 °C.

Zebrafish culture

Zebrafish were maintained and handled in compliance with the local animal welfare regulations as overseen by the Animal Welfare Body of Leiden University (license number: 10612). All practices involving zebrafish were performed in accordance with European laws, guidelines and policies for animal experimentation, housing, and care (European Directive 2010/63/EU on the protection of animals used for scientific purposes). The present study did not involve any procedures within the meaning of Article 3 of Directive 2010/63/EU and as such is not subject to authorization by an ethics committee. Zebrafish lines (Supplementary Table S4) were maintained according to standard protocols (www.zfin.org). Zebrafish eggs were obtained by natural spawning of single crosses to achieve synchronized developmental timing. Eggs from at least 5 couples were combined to achieve heterogeneous groups. Eggs and embryos were kept in egg water (60 µg/ml sea salt, Sera Marin, Heinsberg, Germany) at ~28.5 °C after harvesting and in embryo medium after infection and/or treatment (E2, buffered medium, composition: 15 mM NaCl, 0.5mM KCl, 1 mM MgSO¬4, 150 µM KH2PO4, 1 mM CaCl2 and 0.7 mM NaHCO3) at ~28.5 °C for the duration of experiments.

Bacterial cultures

mWasabi-or mCherry- expressing *Mm* M-strain[65,66] were cultured in Difco Middlebrook 7H9 broth (Becton Dickinson, Breda, the Netherlands) supplemented with 10% ADC (Becton Dickinson), 0.05% Tween 80 (Sigma-Aldrich) and 50 µg/ml Hygromycin B (Life Technologies-Invitrogen) at ~28.5 °C as previously described[52].

Bacterial infection of zebrafish embryos

Fresh *Mm* inoculum was prepared for every infection experiment as described above. The final inoculum was resuspended in PBS containing 2% (w/v) polyvinylpyrrolidone (PVP40). The injection dose was determined by optical density measurement (OD_{600} of 1 corresponds to ~100 CFU/nl). Infection experiments were carried out according to previously described procedures[52]. In brief, microinjections were performed using borosilicate glass microcapillary injection needles (Harvard Apparatus, 300038, 1mm O.D. x 0.78mm I.D.) prepared using a micropipette puller device (Sutter Instruments Flaming/Brown P-97). Needles were mounted on a micromanipulator (Sutter Instruments MM-33R) positioned under a stereo microscope. Prior to injection embryos were anesthetized using 200 µg/ml buffered 3-aminobenzoid acid (Tricaine, Sigma-Aldrich) in egg water. They were then positioned on a 1% agarose plate (in egg water) and injected with an 1 nL inoculum containing ~200 CFU *Mm* at 30 hpf in the blood island or at 3 dpf in the tail fin[45]. For assessment of bacterial burden, larvae were anesthetized using tricaine at 4 days post infection (dpi), positioned on a 1% agarose (in egg water) plate and imaged using a Leica M205 FA stereo fluorescence microscope equipped with a DFC345 FX monochrome camera. Bacterial burden was determined based on fluorescent pixel quantification (Stoop 2011). For confocal imaging larvae were either fixed in 4% paraformaldehyde in PBS at 20°C for 2hrs or at 4°C or anesthetized using tricaine and embedded in 1.5% low melting point agarose (in egg water) before imaging[45]. Timepoints of all confocal experiments are described in the figure legends.

Chemical compound treatments
Treatment of zebrafish embryos was performed by immersion. Stock concentrations were diluted to treatment doses in complete embryo medium without antibiotics. As a solvent control treatment, 100% DMSO was diluted to the same concentration as the compound treatment. If different compound treatment doses were used in the same zebrafish embryo experiment, the solvent control concentration corresponding to the highest compound treatment dose was used. Precise doses of compound treatments and solvent control concentrations as well as the durations of treatment are described in the figure legends for each individual experiment.

Liquid bacterial growth assay
Mm culture in logarithmic growth phase was diluted to an OD_{600} of 0.1 in complete 7H9 broth, of which 5 ml in a T25 Haynes culture flask was incubated with Amiodarone or DMSO at equal v/v at indicated concentrations. *Mm* growth was measured at 2, 6, 24 and 48 hours of incubation at ~28.5°C

Immunostaining
Immunohistochemistry was performed on fixed larvae using a rabbit polyclonal anti-nitrotyrosine antibody (Merck Milipore 06-284 MA, USA) at a 1:200 dilution of the primary antibody, the primary antibody was detected using an Alexa Fluor (Invitrogen Life Technologies NY, USA) secondary antibody in a 1:500 dilution as previously described[33].

Immunostaining imaging
For visualization of fixed 4 dpf uninfected or 1 dpi infected larvae were embedded in 1.5% low melting point agarose (weight per volume, in egg water) and imaged using a Leica TCS SPE confocal 63x oil immersion objective (HC PL APO CS2, NA 1.42) and a Leica TCS SP8 confocal microscope with a 40x water immersion objective (HCX APO L U-V-I, NA 0.8). Corrected total cell fluorescence in figure 2 was calculated using Fiji (version 1.53c) by using measurements for each individual immune-stained cell as previously described[33]. Dedicated image analysis software (Imaris, Bitplane) was used to calculate total signal intensity, normalized total cell fluorescence, volumes and co-localization in figure 3 and 4. Using Imaris, surfaces were made for the different fluorescent channels that were observed and the surface was made to fit the signal as best as possible. By masking the α-nitrotyrosine channel an estimation for background fluorescence was made. Additionally, volumes of observed macrophages were used to correct for cell size. For analysis, the total α-nitrotyrosine signal was used, divided by the volume of the cell and then divided again through the mean intensity.

GFP-Lc3 and LysoTracker imaging
For visualization of Lc3 dynamics, fixed Tg(CMV:EGFP-map1lc3b) larvae were embedded in 1.5% low melting point agarose (weight per volume, in egg water) and imaged using a Leica TCS SPE confocal microscope. Imaging was performed using a 63x oil immersion objective (HC PL APO CS2, NA 1.42) in a region of the tail fin to detect EGFP-map1lc3b – further referred as GFP-Lc3 – positive vesicles. To determine colocalization between *Mm* and GFP-Lc3 fixed larvae were embedded in 1.5% low melting agarose (in egg water) and imaged in the caudal hematopoietic tissue, using a Leica TCS SP8 confocal microscope with a 40x water immersion objective (HCX APO L U-V-I, NA 0.8). For quantification of acidic vesicles, larvae were immersed in embryo medium containing 5 µM LysoTracker Red DND-99 solution (ThermoFisher Scientific) for 1 hour. Before mounting and imaging, larvae were washed 3 times with embryo medium. Live larvae embedded in 1.5% low melting point agarose (weight per volume, in egg water) and imaged using a Leica TCS SP8 confocal microscope. Imaging was performed using a

63x oil immersion objective (HC PL APO CS2, NA 1.40) in a region of the tail fin to detect acidic vesicles. Images were obtained using Leica Las X software. For the quantification of GFP-Lc3 or LysoTracker levels the find maxima algorithm with a noise tolerance of 50 was used in Fiji software version 1.53c. To determine association of GFP-Lc3 with bacteria, manual counting was performed on the obtained confocal images using Leica Las X software.

Tail amputation of zebrafish larvae

Embryos of an Tg(mpeg1:mcherryF)/Tg(mpx;gfp) double transgenic line were anesthetized using tricaine at 3 days post fertilization (dpf), positioned on a 1% agarose (in egg water) plate and the tails were partially amputated with a 1 mm sapphire blade (World Precision Instruments) under a Leica M165C stereomicroscope[67]. After amputation larvae were incubated in embryo medium for 4 hours and fixed using 4% paraformaldehyde. After fixation, larvae were positioned on a 1% agarose (in egg water) plate and imaged using a Leica M205 FA stereo fluorescence microscope equipped with a DFC345 FX monochrome camera. Macrophages were detected based on the fluorescence of their mCherry label and neutrophils were detected based on their GFP label. The number of leukocytes recruited to the wounded area were counted as described previously[67].

RNA isolation, sequencing and sequencing data analysis

Amiodarone treatment of zebrafish larvae was performed from 1 hour post infection (hpi) until 2 dpi (3 dpf). Next, larvae were collected (10 per sample) in QIAzol lysis reagent (Qiagen, Hilden, Germany) and RNA was isolated using miRNeasy mini kit (Qiagen, Hilden, Germany) according to the manufacturer's instructions. RNA integrity was assessed by Bioanalyzer (Agilent, Santa Clara, US) and all samples were found to have a RIN ≥ 9.5. Of the total RNA, 3µg was used to create RNAseq libraries using the Illumina TruSeq strand-specific mRNA polyA preparation kit (Illumina, San Diego, US). The resulting RNAseq library was sequenced for at least 10 million reads per sample using an Illumina HiSeq2500 with a read length of 1 × 50 nucleotides (Baseclear, Leiden, The Netherlands). Four biological replicates for each treatment and infection regime were sequenced and mapped and quantified against the D. rerio GRCzv11 using Salmon v0.14.1[68]. Downstream analysis of the quantified libraries was performed in RStudio 1.2.5001[69] running R 3.6.1[70]. Libraries were imported using tximport v.1.12.3[71]. Differential gene expression was assessed via pairwise comparisons using DESeq2 v1.24.0[72] following a linear model taking into account possible gene expression differences from the embryo parents, drug treatments, infections, and its interaction (design: ~genotype + treatment + infection + treatment:infection). Statistical significance was defined by s-value ≤ 0.005 using apeglm[73]. S-values are aggregate statistics that have been recently proposed as an alternative to adjusted p-value and false discovery rate (FDR), calculating the probability of getting the sign of an effect wrong in biological contexts[74].

Venn Diagram and enrichment analysis, including pathway and GO analysis as well as Gene Set Enrichment Analysis with the C2 "Curated Gene Sets" and C5 "GO Gene Sets" collections from the Molecular Signatures Database (MSigDB) were performed as previously described[75]. Raw data are deposited into the Gene Expression Omnibus under accession number GSE178919. The data and code to recapitulate all figures and findings in this manuscript are available at https://github.com/gabrifc/rnaseq-tamox-amio.

Data analysis and statistics

Mann-Whitney test or Kruskal-Wallis with Dunn's multiple comparisons test was applied when assessing differences between 2 or more groups, respectively, of unpaired data representing technical replicates. Data were normalized to the mean of the control group

and independent repeats were combined, unless otherwise indicated. The number of experiments combined is indicated in the figure legend for each experiment. With exception of the transcriptome profiling analysis, all analyses were performed using GraphPad Prism 8 and the statistical test performed for each experiment is described in the figure legend. Dot plot graphs of zebrafish experiments were made using the raincloud plots application at https://gabrifc.shinyapps.io/raincloudplots[76].

Acknowledgements

We gratefully acknowledge Amy de Waal, Daniel C.M. van der Hoeven and Elisa van der Sar from the Institute of Biology Leiden, Leiden University for their assistance in the experimental work that provided data used in this manuscript.

This project was funded by NWO Domain Applied and Engineering Sciences (NWO-TTW grant 13259) and the Horizon2020 European Marie Skłodowska-Curie programme (fellowship H2020-COFUND-2015-FP-707404). The funders had no role in study design, data collection and analysis, decision to publish, or preparation of the manuscript. The authors declare that they have no conflicting interests.

References

1. Vergne, I., Gilleron, M. & Nigou, J. Manipulation of the endocytic pathway and phagocyte functions by Mycobacterium tuberculosis lipoarabinomannan. *Front. Cell. Infect. Microbiol.* **4**, 1–9 (2015).

2. Levitte, S. *et al.* Mycobacterial Acid Tolerance Enables Phagolysosomal Survival and Establishment of Tuberculous Infection In Vivo. *Cell Host Microbe* **20**, 250–258 (2016).

3. Pires, D. *et al.* Role of Cathepsins in Mycobacterium tuberculosis Survival in Human Macrophages. *Sci. Rep.* **6**, 1–13 (2016).

4. Ramakrishnan, L. Revisiting the role of the granuloma in tuberculosis. *Nat. Rev. Immunol.* **12**, 352–366 (2012).

5. Boshoff, H. I. M. & Barry, C. E. Tuberculosis — metabolism and respiration in the absence of growth. *Nat. Rev. Microbiol. 2005 31* **3**, 70–80 (2005).

6. Friedrich, N., Hagedorn, M., Soldati-Favre, D. & Soldati, T. Prison Break: Pathogens' Strategies To Egress from Host Cells. *Microbiol. Mol. Biol. Rev.* **76**, 707–720 (2012).

7. WHO. *Global Tuberculosis Report 2020*. (2020).

8. Hawn, T. R., Matheson, A. I., Maley, S. N. & Vandal, O. Host-directed therapeutics for tuberculosis: can we harness the host? *Microbiol. Mol. Biol. Rev.* **77**, 608–27 (2013).

9. Tobin, D. M. Host-Directed Therapies for Tuberculosis. *Cold Spring Harb. Perspect. Med.* **5**, a021196 (2015).

10. Wallis, R. S. & Hafner, R. Advancing host-directed therapy for tuberculosis. *Nat. Rev. Immunol.* 1–9 (2015) doi:10.1038/nri3813.

11. Zumla, A., Rao, M., Dodoo, E. & Maeurer, M. Potential of immunomodulatory agents as adjunct host-directed therapies for multidrug-resistant tuberculosis. *BMC Med.* **14**, 1–12 (2016).

12. Kilinç, G., Saris, A., Ottenhoff, T. H. M. & Haks, M. C. Host-directed therapy to combat mycobacterial infections*. *Immunological Reviews* vol. 301 62–83 (2021).

13. Zhang, L. *et al.* Small molecule regulators of autophagy identified by an image-based high-throughput screen. *Proc. Natl. Acad. Sci. U. S. A.* **104**, 19023–19028 (2007).

14. Balgi, A. D. *et al.* Screen for chemical modulators of autophagy reveals novel therapeutic inhibitors of mTORC1 signaling. *PLoS One* **4**, (2009).

15. Jacquin, E. *et al.* Pharmacological modulators of autophagy activate a parallel noncanonical pathway driving unconventional LC3 lipidation. *Autophagy* **13**, 854–867 (2017).

16. Yang, Z. & Klionsky, D. J. Mammalian autophagy: Core molecular machinery and signaling regulation. *Curr. Opin. Cell Biol.* **22**, 124–131 (2010).

17. Deretic, V., Saitoh, T. & Akira, S. Autophagy in infection, inflammation and immunity. *Nat. Rev. Immunol.* **13**, 722–37 (2013).

18. Stadler, K. *et al.* Amiodarone alters late endosomes and inhibits SARS coronavirus infection at a post-endosomal level. *Am. J. Respir. Cell Mol. Biol.* **39**, 142–149 (2008).

19. Kishida, S. *et al.* Amiodarone and N-desethylamiodarone enhance endothelial nitric oxide production in human endothelial cells. *Int. Heart J.* **47**, 85–93 (2006).

20. Bogdan, C. Nitric oxide and the immune response. *Nature Immunology* vol. 2 907–916 (2001).

21. Gutierrez, M. G. *et al.* Autophagy is a defense mechanism inhibiting BCG and Mycobacterium tuberculosis survival in infected macrophages. *Cell* **119**, 753–766 (2004).

22. Bradfute, S. B. *et al.* Autophagy as an immune effector against tuberculosis. *Curr. Opin. Microbiol.* **16**, 355–365 (2013).

23. Fleming, A., Noda, T., Yoshimori, T. & Rubinsztein, D. C. Chemical modulators of autophagy as biological probes and potential therapeutics. *Nat. Chem. Biol.* **7**, 9–17 (2011).

24. Noda, T. & Ohsumi, Y. Tor, a phosphatidylinositol kinase homologue, controls autophagy in yeast. *J. Biol. Chem.* **273**, 3963–3966 (1998).

25. Sarkar, S., Ravikumar, B., Floto, R. A. & Rubinsztein, D. C. Rapamycin and mTOR-independent autophagy inducers ameliorate toxicity of polyglutamine-expanded huntingtin and related proteinopathies. *Cell Death Differ.* **16**, 46–56 (2009).

26. Mizushima, N. *et al.* Dissection of autophagosome formation using Apg5-deficient mouse embryonic stem cells. *J. Cell Biol.* **152**, 657–667 (2001).

27. Peranzoni, E. *et al.* Role of arginine metabolism in immunity and immunopathology. *Immunobiology* **212**, 795–812 (2008).

28. Adams, L. B., Dinauer, M. C., Morgenstern, D. E. & Krahenbuhl, J. L. Comparison of the roles of reactive oxygen and nitrogen intermediates in the host response to Mycobacterium tuberculosis using transgenic mice. *Tuber. Lung Dis.* **78**, 237–246 (1997).

29. GS, J., HJ, A. & BR, A. Killing of Mycobacterium tuberculosis by neutrophils: a nonoxidative process. *J. Infect. Dis.* **162**, 700–704 (1990).

30. WU, G. & MORRIS, S. M. Arginine metabolism: nitric oxide and beyond. *Biochem. J.* **336**, 1–17 (1998).

31. Yang, C.-S., Yuk, J.-M. & Jo, E.-K. The Role of Nitric Oxide in Mycobacterial Infections. *Immune Netw.* **9**, 46 (2009).

32. Voskuil, M. I., Bartek, I. L., Visconti, K. & Schoolnik, G. K. The response of Mycobacterium tuberculosis to reactive oxygen and nitrogen species. *Front. Microbiol.* **2**, 1–12 (2011).

33. Elks, P. M. *et al.* Hypoxia Inducible Factor Signaling Modulates Susceptibility to Mycobacterial Infection via a Nitric Oxide Dependent Mechanism. *PLoS Pathog.* **9**, 1–16 (2013).

34. Ramakrishnan, L. The Zebrafish Guide to Tuberculosis Immunity and Treatment. *Cold Spring Harb. Symp. Quant. Biol.* **78**, 179–192 (2013).

35. Meijer, A. H. Protection and pathology in TB: learning from the zebrafish model. *Semin. Immunopathol.* **38**, 261–273 (2016).

36. Davis, J. M. *et al.* Real-time visualization of Mycobacterium-macrophage interactions leading to initiation of granuloma formation in zebrafish embryos. *Immunity* **17**, 693–702 (2002).

37. van der Vaart, M. *et al.* The DNA Damage-Regulated Autophagy Modulator DRAM1 Links Mycobacterial Recognition via TLR-MYD88 to Autophagic Defense. *Cell Host Microbe* **15**, 753–767 (2014).

38. Zhang, R. *et al.* The selective autophagy receptors Optineurin and p62 are both required for zebrafish host resistance to mycobacterial infection. *PLOS Pathog.* **15**, e1007329 (2019).

39. Renshaw, S. a *et al.* A transgenic zebrafish model of neutrophilic inflammation. *Blood* **108**, 3976–8 (2006).

40. Xie, Y., Meijer, A. H. & Schaaf, M. J. M. Modeling Inflammation in Zebrafish for the Development of Anti-inflammatory Drugs. *Front. Cell Dev. Biol.* **8**, (2021).

41. Lambeth, J. D. NOX enzymes and the biology of reactive oxygen. *Nat. Rev. Immunol.* **4**, 181–189 (2004).

42. Elks, P. M. *et al.* Mycobacteria Counteract a TLR-Mediated Nitrosative Defense Mechanism in a Zebrafish Infection Model. *PLoS One* **9**, e100928 (2014).

43. Elks, P. M., Renshaw, S. a., Meijer, a. H., Walmsley, S. R. & van Eeden, F. J. Exploring the HIFs, buts and maybes of hypoxia signalling in disease: lessons from zebrafish models. *Dis. Model. Mech.* **8**, 1349–1360 (2015).

44. He, C., Bartholomew, C. R., Zhou, W. & Klionsky, D. J. Assaying autophagic activity in transgenic GFP-Lc3 and GFP-Gabarap zebrafish embryos. *Autophagy* **5**, 520–526 (2009).

45. Hosseini, R. *et al.* Correlative light and electron microscopy imaging of autophagy in a zebrafish infection model. *Autophagy* **10**, 1844–1857 (2014).

46. Benard, E. L., Rougeot, J., Racz, P. I., Spaink, H. P. & Meijer, A. H. *Transcriptomic Approaches in the Zebrafish Model for Tuberculosis—Insights Into Host- and Pathogen-specific Determinants of the Innate Immune Response*. *Advances in Genetics* vol. 95 (Elsevier Ltd, 2016).

47. AG, W. & HC, C. Amiodarone-Associated Optic Neuropathy: Clinical Review. *Neuroophthalmology.* **41**, 55–58 (2016).

48. Alshehri, M. & Joury, A. Ocular Adverse Effects of Amiodarone: A Systematic Review of Case Reports. *Optom. Vis. Sci.* **97**, 536–542 (2020).

49. M, G., D, D. & W, K. Amiodarone causes endothelium-dependent vasodilation in human hand veins in vivo. *Clin. Pharmacol. Ther.* **64**, 302–311 (1998).

50. Gomes, L. C. & Dikic, I. Autophagy in antimicrobial immunity. *Mol. Cell* **54**, 224–233 (2014).

51. Lieschke, G. J. & Currie, P. D. Animal models of human disease: Zebrafish swim into view. *Nat. Rev. Genet.* **8**, 353–367 (2007).

52. Benard, E. L. *et al.* Infection of zebrafish embryos with intracellular bacterial pathogens. *J. Vis. Exp.* 1–8 (2012) doi:10.3791/3781.

53. Cui, C. *et al. Infectious disease modeling and innate immune function in zebrafish embryos. Methods in cell biology* vol. 105 (Elsevier Inc., 2011).

54. Gefter, W. B., Epstein, D. M., Pietra, G. G. & Miller, W. T. Lung disease caused by amiodarone, a new antiarrythmic agent. *Radiology* **147**, 339–344 (1983).

55. Papiris, S. A., Triantafillidou, C., Kolilekas, L., Markoulaki, D. & Manali, E. D. Amiodarone: Review of pulmonary effects and toxicity. *Drug Saf.* **33**, 539–558 (2010).

56. Karinauske, E. *et al.* A case report and literature review: Previously excluded tuberculosis masked by amiodarone induced lung injury. *BMC Pharmacol. Toxicol.* **19**, 1–6 (2018).

57. Keller, M. D., Torres, V. J. & Cadwell, K. Autophagy and microbial pathogenesis. *Cell Death Differ.* **27**, 872–886 (2020).

58. Aimo, A., Baritussio, A., Emdin, M. & Tascini, C. Amiodarone as a possible therapy for coronavirus infection. *Eur. J. Prev. Cardiol.* 3–5 (2020) doi:10.1177/2047487320919233.

59. Berg, R. D. *et al.* Lysosomal Disorders Drive Susceptibility to Tuberculosis by Compromising Macrophage Migration. *Cell* **165**, 139–152 (2016).

60. Buratta, S. *et al.* A role for the autophagy regulator Transcription Factor EB in amiodarone-induced phospholipidosis. *Biochem. Pharmacol.* **95**, 201–209 (2015).

61. SPYROPOULOS, B. Tay-Sachs carriers and tuberculosis resistance. *Nature* **331**, 666–666 (1988).

62. Meijer, A. H. & Aerts, J. M. Linking Smokers' Susceptibility to Tuberculosis with Lysosomal Storage Disorders. *Dev. Cell* **37**, 112–113 (2016).

63. Sommer, F. *et al.* Disruption of Cxcr3 chemotactic signaling alters lysosomal function and renders macrophages more microbicidal. *Cell Rep.* **35**, 109000 (2021).

64. Bolt, M. W., Card, J. W., Racz, W. J., Brien, J. F. & Massey, T. E. Disruption of mitochondrial function and cellular ATP levels by amiodarone and N-desethylamiodarone in initiation of amiodarone-induced pulmonary cytotoxicity. *J. Pharmacol. Exp. Ther.* **298**, 1280–9 (2001).

65. van der Sar, A. M. *et al.* Mycobacterium marinum Strains Can Be Divided into Two Distinct Types Based on Genetic Diversity and Virulence. *Infect. Immun.* **72**, 6306–6312 (2004).

66. Takaki, K., Davis, J. M., Winglee, K. & Ramakrishnan, L. Evaluation of the pathogenesis and treatment of Mycobacterium marinum infection in zebrafish. *Nat. Protoc.* **8**, 1114–24 (2013).

67. Xie, Y. *et al.* Glucocorticoids inhibit macrophage differentiation towards a pro-inflammatory phenotype upon wounding without affecting their migration. *Dis. Model. Mech.* **12**, dmm037887 (2019).

68. Patro, R., Duggal, G., Love, M. I., Irizarry, R. A. & Kingsford, C. Salmon provides fast and bias-aware quantification of transcript expression. *Nat. Methods* **14**, 417–419 (2017).

69. RStudio Team. RStudio: Integrated Development for R. RStudio, PBC, Boston, MA. http://www.rstudio.com/ (2020).

70. R Core Team. R: a language and environment for statistical computing. https://www.r-project.org/ (2018).

71. Soneson, C., Love, M. I. & Robinson, M. D. Differential analyses for RNA-seq: Transcript-level estimates improve gene-level inferences. *F1000Research* **4**, (2016).

72. Love, M. I., Huber, W. & Anders, S. Moderated estimation of fold change and dispersion for RNA-seq data with DESeq2. *Genome Biol. 2014 1512* **15**, 1–21 (2014).

73. Zhu, A., Ibrahim, J. G. & Love, M. I. Heavy-tailed prior distributions for sequence count data: removing the noise and preserving large differences. *Bioinformatics* **35**, 2084–2092 (2019).

74. Stephens, M. False discovery rates: A new deal. *Biostatistics* **18**, 275–294 (2017).

75. Zhang, R. *et al.* Deficiency in the autophagy modulator Dram1 exacerbates pyroptotic cell death of Mycobacteria-infected macrophages. *Cell Death Dis. 2020 114* **11**, 1–16 (2020).

76. Allen, M. *et al*. Raincloud plots: a multi-platform tool for robust data visualization [version 2; peer review: 2 approved]. *Wellcome Open Res. 2021 463* **4**, 63 (2021).

Supplementary data and tables

Supplementary Data Table 1 can be downloaded via https://doi.org/10.5281/zenodo.5788771.

Gene name	Ensembl ID	s-value (CTRL)	Log2FC (CTRL)	s-value (AMIO)	Log2FC (AMIO)
c4b	ENSDARG00000038424	1,32E-26	1,41242232	0,000426874	0,427846742
cd63	ENSDARG00000115979	0,000783028	0,22990061	0,001721136	0,208615745
cfb	ENSDARG00000110358	6,77E-22	1,91084473	3,41E-07	0,968397619
cp	ENSDARG00000010312	2,55E-13	0,68712585	0,002866682	0,248472345
ctsc	ENSDARG00000101334	9,22E-07	0,58292046	7,99E-07	0,584656237
lgals9l1	ENSDARG00000025903	3,41E-12	1,86780544	3,14E-18	2,375554832
ncf1	ENSDARG00000033735	2,53E-09	1,29881729	6,10E-06	0,974733487
stat3	ENSDARG00000022712	0,003413588	0,22468678	0,000147126	0,301455165
tcirg1b	ENSDARG00000105142	1,52E-08	0,54863188	0,002278049	0,27273832
zmp:0000001082	ENSDARG00000098899	1,71E-07	0,81669974	0,000365082	0,559371158

Supplementary table S1. Effect of treatment and infection on gene regulation

Gene name	Ensembl ID	s-value	Log2FC
ccnd2a	ENSDARG00000051748	0,001758206	-0,6694574
cfb	ENSDARG00000110358	0,001164028	-0,8979486
CU682777.1	ENSDARG00000054207	0,001960381	-2615936
gas7a	ENSDARG00000111294	0,003391572	0,9261403
gdpd5a	ENSDARG00000077284	0,001496878	0,6968877
lin54	ENSDARG00000063194	0,000190726	-0,8305882
moxd1	ENSDARG00000031136	0,004379886	-0,7649399
nbas	ENSDARG00000008593	0,004773179	-0,604494091
ncf1	ENSDARG00000033735	0,002231734	-0,9422264
nudt4a	ENSDARG00000057767	0,002677158	-0,4509043
otub1b	ENSDARG00000011462	0,003079944	0,383625054
rell2	ENSDARG00000071876	0,00074083	-1547236
si:cabz01007802.1	ENSDARG00000068030	0,003692912	-0,7809593
tyw1	ENSDARG00000062987	0,003988326	0,4300815
vps26b	ENSDARG00000015823	0,002448688	-0,672679549
zgc:158328	ENSDARG00000005216	0,002892983	-0,764794573

Supplementary table S2. Interaction of treatment and infection on gene regulation

KEGG pathway		
Pathway	**Number of DR genes**	**padj**
Metabolic pathways	66 (out of 1458)	0,000
Lysosome	20 (out of 140)	0,000
Metabolism of xenobiotics by cytochrome P450	11 (out of 35)	0,000
Drug metabolism - other enzymes	13 (out of 62)	0,000
Glutathione metabolism	11 (out of 57)	0,000
Drug metabolism - cytochrome P450	9 (out of 32)	0,000
Other glycan degradation	7 (out of 24)	0,000
Phagosome	13 (out of 142)	0,000
Phototransduction	7 (out of 37)	0,000
Porphyrin and chlorophyll metabolism	6 (out of 28)	0,000
Amino sugar and nucleotide sugar metabolism	7 (out of 57)	0,001
Histidine metabolism	5 (out of 25)	0,001
Ferroptosis	6 (out of 41)	0,001
Ascorbate and aldarate metabolism	4 (out of 17)	0,002
Retinol metabolism	5 (out of 38)	0,004
Purine metabolism	9 (out of 151)	0,009

Gene Ontology (GoSeq)				
GO term	**Category**	**Ontology**	**Number of DR genes**	**p-adj**
transferase activity, transferring hexosyl groups	GO:0016758	MF	10 (out of 66)	0,000138178
oxidation-reduction process	GO:0055114	BP	35 (out of 891)	0,000138178
lysosome	GO:0005764	CC	10 (out of 74)	0,000141739
visual perception	GO:0007601	BP	12 (out of 119)	0,000141739
glucuronosyltransferase activity	GO:0015020	MF	8 (out of 39)	0,000165387
glutathione transferase activity	GO:0004364	MF	6 (out of 22)	0,000179239
photoreceptor activity	GO:0009881	MF	7 (out of 43)	0,001788054
oxidoreductase activity	GO:0016491	MF	25 (out of 610)	0,00280307
proton-transporting V-type ATPase, V1 domain	GO:0033180	CC	5 (out of 17)	0,002853676
hydrolase activity	GO:0016787	MF	40 (out of 1268)	0,002853676
iron ion binding	GO:0005506	MF	13 (out of 203)	0,00469861
catalytic activity	GO:0003824	MF	24 (out of 587)	0,00469861
oxidoreductase activity [...]	GO:0016705	MF	11 (out of 143)	0,005523145
carbohydrate metabolic process	GO:0005975	BP	13 (out of 208)	0,005646846
phototransduction	GO:0007602	BP	6 (out of 41)	0,007918938
protein-chromophore linkage	GO:0018298	BP	6 (out of 41)	0,007918938
ATP hydrolysis coupled proton transport	GO:0015991	BP	6 (out of 39)	0,007941036

Supplementary table S3. KEGG pathway and Gene Ontology (GoSeq) analysis

Zebrafish lines		
Name	**Description**	**Reference**
AB/TL	Wild type strain	Zfin.org
Tg(CMV:EGFP-map1lc3b)^{zf155}	GFP-tagged zebrafish Lc3	He 2009
Tg(mpeg1:mCherryF)^{umsF001}	Macrophage marker	Bernut 2014
Tg(mpeg1:EGFP)^{gl22}	Macrophage marker	Ellett 2011
Tg(mpx:EGFP)^{i114}	Neutrophil marker	Renshaw 2006
Tg(mpeg1:mCherryF, mpx:EGFP)$^{umsF001, i114}$	Macrophage and neutrophil marker	Bernut 2014, Renshaw 2006

Supplementary table S4. Supplementary materials